J Stat Phys (2010) 138: 51–84
DOI 10.1007/s10955-010-9924-9

Phase Separation in Confined Geometries

Kurt Binder · Sanjay Puri · Subir K. Das · Jürgen Horbach

Received: 16 October 2009 / Accepted: 8 January 2010 / Published online: 4 February 2010

Abstract The kinetics of phase separation or domain growth, subsequent to temperature quenches of binary mixtures from the one-phase region into the miscibility gap, still remains a challenging problem of nonequilibrium statistical mechanics. We have an incomplete understanding of many aspects of the growth of concentration inhomogeneities, including the effect of surfaces on this process, and the interplay with wetting phenomena and finite-size effects in thin films. In the present paper, an overview of the simulation approaches to this problem is given, with an emphasis on solutions of a diffusive Ginzburg-Landau model. We also discuss two recent alternative approaches: a local molecular field approximation to the Kawasaki spin exchange model on a lattice; and molecular dynamics simulations of a fluid binary Lennard-Jones mixture. A brief outlook to open questions is also given.

Keywords Domain growth · Ginzburg-Landau theory · Molecular dynamics simulation · Thin films · Surface-directed spinodal decomposition

1 Introduction

There has been intense research interest in the *kinetics of phase transitions*. In this context, consider a binary (AB) mixture which is homogeneous at high temperatures. This system

K. Binder
Institut für Physik, Johannes Gutenberg—Universität Mainz, 55099 Mainz, Germany

S. Puri
School of Physical Sciences, Jawaharlal Nehru University, New Delhi 110067, India

S.K. Das
Theoretical Sciences Unit, Jawaharlal Nehru Centre for Advanced Scientific Research, Jakkur, Bangalore 560064, India

J. Horbach (✉)
Institut für Materialphysik im Weltraum, Deutsches Zentrum für Luft- und Raumfahrt (DLR), 51170 Köln, Germany
e-mail: juergen.horbach@dlr.de

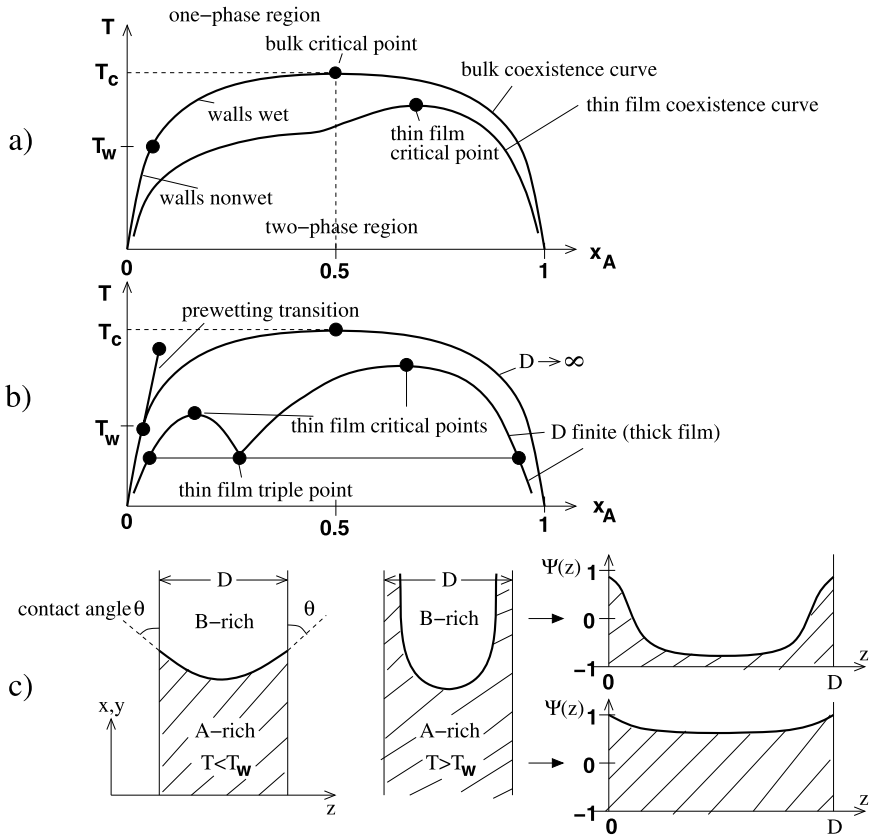

Fig. 1 Schematic phase diagrams (**a**), (**b**) and corresponding states (**c**) of a symmetric AB mixture in a thin film of thickness D. The film is symmetric, viz., both walls attract the A-particles with the same strength. The wetting transition only occurs in the limit $D \to \infty$. For finite D, the transition of the walls from nonwet or partially wet to wet or completely wet is rounded off. This transition is of second order in (**a**), while (**b**) refers to a first-order wetting transition. In (**b**), a prewetting transition line exists in the one-phase region, with one end being a prewetting critical point at high temperatures. The other end of this line is at the wetting transition temperature T_w, at the coexistence curve that separates the two-phase region from the one-phase region. Note that the critical concentration of a symmetric binary mixture is $x_A^{crit} = 0.5$ in the bulk, but is shifted to a larger value x_A in the thin film. Further, the critical temperature of the film is typically lower than in the bulk, $T_c(D) < T_c(\infty) = T_c$. For the case of first-order wetting and sufficiently large D, a thin-film analog of the prewetting transition exists, as evidenced by the thin-film critical point at the left side of the phase diagram. When the thin enrichment layer segregation meets the lateral segregation of the thick film, a thin-film triple point occurs at a temperature close to T_w. For thin films, this triple point and the left critical point may merge and annihilate each other, and the corresponding phase diagram is similar to that in (**a**). In (**c**), we provide schematic pictures of the thin-film states in the case of lateral phase separation

becomes thermodynamically unstable if it is rapidly quenched below the coexistence curve [see Fig. 1(a)]. The subsequent evolution of the system is characterized by the emergence and growth of domains which are A-rich and B-rich. This evolution is termed *domain growth* or *coarsening* or *phase ordering dynamics*. Typically, a characteristic length scale $L(t)$ appears during the late stages of this process. In many cases, there is a power-law increase of this length scale with the time t after the quench, and associated scaling behavior is observed. The asymptotic state of the system is the equilibrium phase-separated state, which

reflects the initial composition of the mixture. These kinetic processes are of great scientific and technological importance. There now exists a good understanding of the kinetics of phase separation in the bulk, and there are several good reviews of these problems [1–5].

Next, let us consider a binary mixture in contact with a surface S. In many physical applications, the surface has a preferential attraction for one of the components of the mixture, say A. In equilibrium, the AB interface meets the wall at a contact angle θ, which is determined by Young's equation [6]:

$$\sigma \cos\theta = \gamma_B - \gamma_A. \tag{1}$$

Here, σ is the surface tension between the A-rich and B-rich phases; and γ_A, γ_B are the surface tensions between the A-rich and B-rich phases and S, respectively. For $\sigma > \gamma_B - \gamma_A$, the surface is *partially wet* (PW) in equilibrium. For $\sigma < \gamma_B - \gamma_A$, (1) has no solution and the A-rich phase forms a macroscopic layer on the surface in a *completely wet* (CW) morphology [7–11]. The above picture applies for a semi-infinite geometry—only precursors of wetting layers are possible in a confined geometry, e.g., thin film with parallel surfaces separated by a distance D (see Fig. 1).

There also has been a long-standing interest in the problem of phase separation in confined geometries [12–18]. The confining surfaces give rise to *surface-directed phase separation* or *surface-directed spinodal decomposition* (SDSD), viz., the dynamical interplay of wetting and phase separation when an unstable binary mixture is placed in contact with a wetting surface. These processes have important technological applications, including the fabrication of layered structures and nanoscale patterns. Even in thin films which are several μm thick, the length scale $L(t)$ mentioned above becomes comparable to the film thickness in the late stages of domain growth, and the finite size and surface effects become important.

The first study of SDSD is due to Jones et al. [15], who studied the segregation of mixtures of poly(ethylenepropylene) (PEP) and perdeuterated-PEP (dPEP). These mixtures had an open surface, which was preferentially wetted by dPEP. Jones et al. observed the formation of SDSD waves which propagated into the bulk with wave-vectors normal to the surface, as shown in Fig. 2. Krausch et al. [16] improved on these experiments, studying a similar system but with better techniques. They focused on the time-dependence of the first "zero"-crossing of the SDSD profiles (see Fig. 2), viz., the distance from the surface [say $R_1(t)$] where the composition first assumes its average value. Their results showed that $R_1(t) \sim t^{1/3}$, which is analogous to the Lifshitz-Slyozov (LS) law for diffusion-driven domain growth in the bulk [5].

We will not discuss experimental results further here, but rather refer the reader to the comprehensive reviews by Krausch [17], and Geoghegan and Krausch [18]. However, these results provide guidance to the relevant theoretical questions which we address here.

In this paper, we review our studies of phase separation in confined geometries. In Sect. 2, we briefly discuss phase-separation kinetics in the bulk. This will provide the background for our discussion of phase separation at surfaces. In Sect. 3, we present our modeling and results for SDSD in a semi-infinite geometry. In Sect. 4, we discuss the kinetics of phase separation in thin films. We conclude this paper with a summary and discussion in Sect. 5.

2 Phase Separation in the Bulk

2.1 Correlation Functions and Structure Factors

Let us start with a brief overview of phase-separation kinetics in bulk mixtures. For quenches below the spinodal curve, the homogeneous system is unstable and decomposes via the

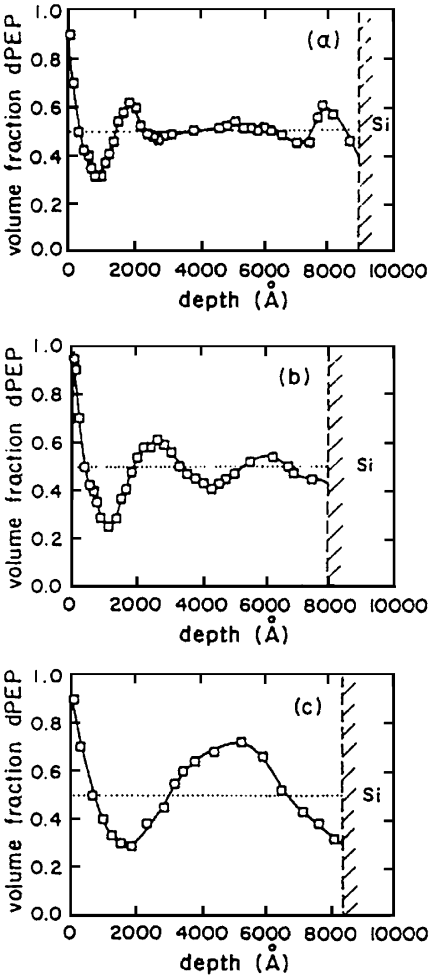

Fig. 2 SDSD in an unstable polymer mixture of PEP and dPEP, in contact with an open surface which prefers dPEP [15]. The frames show the depth-dependence of the volume fraction of dPEP at (**a**) 19200 s, (**b**) 64440 s, and (**c**) 172800 s after the quench. The average composition is denoted by a *dotted line*

spontaneous growth of long-wavelength concentration fluctuations (*spinodal decomposition*) [1–5]. As a caveat, we mention that the concept of a "spinodal curve" is well-defined in a mean-field context only [2, 5]. In fact, for systems with short range forces, the nature of the initial stages of phase separation changes gradually from *spinodal decomposition* to *nucleation and growth* when the considered state point moves from the center of the miscibility gap towards the coexistence curve.

As mentioned earlier, the coarsening domains have a characteristic length scale $L(t)$, which grows with time t. In pure and isotropic systems, domain growth usually obeys power-law growth, $L(t) \sim t^{\phi}$, where ϕ is the growth exponent. If the system is characterized by a single length scale, the morphology of the domains does not change with time, apart from a scale factor. Therefore, the *order-parameter correlation function* exhibits a dynamical-scaling property [1–5]:

$$C(\vec{r},t) \equiv \frac{1}{V}\int d\vec{R}\big[\langle\psi(\vec{R},t)\psi(\vec{R}+\vec{r},t)\rangle - \langle\psi(\vec{R},t)\rangle\langle\psi(\vec{R}+\vec{r},t)\rangle\big]$$
$$= g\left(\frac{r}{L}\right), \tag{2}$$

where V is the system volume, and the angular brackets denote an averaging over independent initial conditions and thermal fluctuations. This equal-time correlation function is a time-dependent quantity as domain growth is a nonequilibrium process. In (2), $g(x)$ is a scaling function which is independent of time.

Actually, most experiments (e.g., neutron or light scattering) probe the *structure factor*, which is the Fourier transform of the correlation function:

$$S(\vec{k},t) = \int d\vec{r} e^{i\vec{k}\cdot\vec{r}} C(\vec{r},t), \tag{3}$$

where $\vec{k}$ is the wave-vector of the scattered beam. The corresponding dynamical-scaling form for $S(\vec{k},t)$ is

$$S(\vec{k},t) = L^d f(kL), \tag{4}$$

where d is the dimensionality, and

$$f(p) = \int d\vec{x} e^{i\vec{p}\cdot\vec{x}} g(x). \tag{5}$$

The scaling functions $g(x)$ and $f(p)$ characterize the morphology of the ordering system. In experiments or simulations of domain growth, one usually attempts to obtain the functional forms of $g(x)$ and $f(p)$. Of course, a complete description of the morphology would require knowledge of all higher-order correlation functions and structure factors also, but these have limited experimental relevance.

2.2 Domain Growth Laws

Next, let us discuss the *domain growth laws* which arise in phase ordering systems [19–26]. The *evaporation-condensation mechanism* of Lifshitz and Slyozov (LS) [19] corresponds to a situation where droplets of the minority phase (say, A) are in local equilibrium with the surrounding supersaturated majority phase. The LS mechanism leads to a growth law $L(t) \propto t^{1/3}$, valid for $d > 1$. Huse [27] demonstrated that the same law is applicable to spinodal decomposition, where there are approximately equal fractions of the two components and the coarsening structure is bi-continuous. Typically, the chemical potential excess (relative to the chemical potential at bulk coexistence) on the surface of a domain of size L is $\mu \sim \sigma/L$, where σ is the surface tension. The concentration current is obtained as $D|\vec{\nabla}\mu| \sim D\sigma/L^2$, where D is the diffusion constant. Therefore, the domain size grows as $dL/dt \sim D\sigma/L^2$, or $L(t) \sim (D\sigma t)^{1/3}$. The LS law applies to phase separation in multicomponent mixtures [28] driven by diffusion, as in solid alloys when strain-field effects can be neglected.

In fluid mixtures, there is a range of mechanisms which drive phase separation. For example, the droplet *diffusion-coagulation mechanism* [25, 26] is based on Stokes law for the diffusion of droplets, and yields a growth law [25, 26] $L(t) \propto (t/\eta)^{1/d}$, where η is the fluid viscosity. A faster mechanism was proposed by Siggia [20], who studied the coarsening of interconnected domain structures in $d = 3$ via the deformation and break-up of tube-like regions. Siggia considered the balance between the surface energy density $\sim \sigma/L$ and the viscous stress $\sim 6\pi\eta v/L$, where v is the magnitude of the fluid velocity [3]. Thus, $v \sim dL/dt \propto \sigma/\eta$ or $L(t) \propto \sigma t/\eta$ in $d = 3$.

In $d = 2$, the analog of the Siggia mechanism is controversial. San Miguel et al. [21] argue that strips ($d = 2$ analogs of tubes) are stable under small perturbations, in contrast to the $d = 3$ case. For critical volume fractions, an *interface diffusion mechanism* is proposed

which yields $L(t) \propto t^{1/2}$, i.e., the same growth law as the diffusion-coagulation mechanism of droplets in $d = 2$ (see above). On the other hand, Furukawa [22, 23] argues for a linear growth law $L(t) \propto t$ in $d = 2$ as well. However, recently there is growing evidence [29–31] that different characteristic length scales in $d = 2$ may exhibit different growth exponents, suggesting that there is no simple dynamical scaling of domain growth in $d = 2$ fluid mixtures.

Finally, we mention that the above growth laws for fluid mixtures do not constitute the true asymptotic behavior, either in $d = 2$ or $d = 3$. Rather, these results only hold for low Reynolds numbers [3, 5]. For $L \gg \eta^2/(\rho\sigma)$ (the so-called inertial length [3, 5]), one enters a regime where the surface-energy density σ/L is balanced by the kinetic-energy density ρv^2. This yields the following growth law for the inertial regime [3, 5, 22, 23]:

$$L(t) \propto \left(\frac{\sigma t^2}{\rho}\right)^{1/3}, \tag{6}$$

which is valid for both $d = 2$ and $d = 3$. In $d = 3$, evidence for both $L(t) \propto t$ and $L(t) \propto t^{2/3}$ has been reported, but the conditions under which such power laws hold in $d = 2$ are still unclear [29–37].

3 Phase Separation in a Semi-Infinite Geometry

3.1 Free Energy for Binary Mixtures at Surfaces

Consider an AB mixture in contact with a planar surface S, located at $z = 0$. The mixture consists of N_A atoms of A and N_B atoms of B distributed on a lattice, with $N = N_A + N_B$. If a lattice site i is occupied by an A-atom or B-atom, we associate the Ising spin variables $\sigma_i = +1$ or $\sigma_i = -1$, respectively.

We consider the case with nearest-neighbor interactions. Furthermore, the interactions are taken to be independent of the sites i and j, except when both of these lie in the surface layer (labeled by $i_z = 1$). The resultant Ising Hamiltonian for the binary mixture is

$$\mathcal{H}\{\sigma_i\} = -\sum_{\langle ij\rangle} J_{ij}\sigma_i\sigma_j - H\sum_{i=1}^{N}\sigma_i - H_1\sum_{i_z=1}\sigma_i + \sum_{i_z>1} V(z_i)\sigma_i, \tag{7}$$

where the pair-wise exchange interaction is

$$\begin{aligned} J_{ij} &= J, \quad i_z \text{ or } j_z \neq 1, \\ &= J_s, \quad i_z, j_z = 1. \end{aligned} \tag{8}$$

Here, the subscript s denotes the surface layer. The bulk "magnetic field" H is irrelevant in the fixed-concentration ensemble where $\sum_i \sigma_i = N_A - N_B$. We distinguish between the surface field $-H_1$ and the "bulk" potential $V(z)$, both of which result from the introduction of a surface. We can have a non-zero H_1 even if $V(z) = 0$, due to missing neighbors for $z < 0$ [12, 13]. Here, we will focus on the simplest case where $-H_1 = V(i_z = 1)$. It is experimentally relevant to consider both short-ranged potentials [$V(z) \sim \delta(z)$ or $V(z) \sim \exp(-z/z_0)$, where z_0 is the characteristic decay length] and long-ranged power-law potentials [$V(z) \sim z^{-n}$]. There are significant differences between wetting by short-ranged and long-ranged potentials [11]. The generalization of the Hamiltonian in (7) to an arbitrary geometry is obvious.

For example, in a thin film of thickness D, the RHS of (7) contains additional terms arising from the surface at $z = D$.

Based on the molecular field approximation of the Hamiltonian in (7), a continuum description for the binary AB mixture at the surface can be obtained, leading to the formulation of a free-energy functional $\mathcal{F}$. The expression for $\mathcal{F}$ includes the usual entropy of mixing. We introduce the order parameter $\langle \sigma_i \rangle = \psi(\vec{r}_i)$, and Taylor-expand around $\vec{r}_i$ to obtain

$$\begin{aligned}\mathcal{F}[\psi] \simeq & \int d\vec{r} \left[-\frac{1}{2} k_B (T_c - T)\psi^2 + \frac{k_B T}{12}\psi^4 + \frac{J}{2}\left(\vec{\nabla}\psi\right)^2 + V(z)\psi \right] \\ & + \int d\vec{\rho} \left\{ -\frac{1}{2}\left[(q-2)J_s + J - k_B T\right]\psi(\vec{\rho},0)^2 - H_1 \psi(\vec{\rho},0) \right. \\ & \left. + \frac{J_s}{2}\left[\vec{\nabla}_{\parallel}\psi(\vec{\rho},0)\right]^2 - \frac{J}{2}\psi(\vec{\rho},0)\frac{\partial\psi}{\partial z}\bigg|_{z=0} \right\} \\ \equiv & \mathcal{F}_b + \mathcal{F}_s. \end{aligned} \tag{9}$$

Here, $\mathcal{F}_b$ is the ψ^4-form of the bulk free energy supplemented by a surface potential term, and $\mathcal{F}_s$ is the surface contribution. We designate $\vec{r} = (\vec{\rho}, z)$, where $\vec{\rho}$ are the $(d-1)$ coordinates parallel to the surface, and z is the coordinate perpendicular to the surface. The critical temperature is denoted as T_c, and the temperature as T. The quantity q denotes the coordination number of a lattice site. The term $\partial\psi/\partial z|_{z=0}$ in $\mathcal{F}_s$ appears because of the missing neighbors for $z < 0$. The expansion which results in (9) is only justifiable near criticality, where the order-parameter amplitude is small. However, we will also use this free energy for parameter values far from criticality. This is reasonable if the resultant model adequately describes experimental phenomenology. The appropriate minimal model for description of surface critical phenomena has been discussed extensively in the literature [38–45].

3.2 Equilibrium Morphologies for a Mixture at a Surface

We are interested in the equilibrium morphologies for a binary mixture at a surface. These are the asymptotic states of the thermodynamically unstable mixture which undergoes SDSD. It is convenient to understand these morphologies in the context of a thin film of thickness D—the limit $D \to \infty$ corresponds to the semi-infinite case (see Fig. 1).

Recall that a homogeneous binary mixture becomes unstable when it is quenched into the miscibility gap. For a symmetric mixture, the miscibility gap is symmetric with respect to the concentration $x_A^{crit} = 1/2$. A semi-infinite mixture at a surface may undergo a wetting transition [10, 11, 38–45]. This transition implies a singular behavior of the surface excess free energy F_s. This is defined as (for a film between two equivalent walls at distance D)

$$F_{film} = F_b + \frac{2F_s}{D}, \quad D \to \infty, \tag{10}$$

F_b being the bulk free energy per unit volume of the system. Assuming, as done in Fig. 1, that the wetting transition occurs at the surface of B-rich mixtures (caused by the preferential attraction of A to the walls), the transition is characterized by a divergence of the surface excess concentration of A, x_A^{surf}. This quantity can be obtained from F_s via suitable derivatives, or by integrating the concentration profile [38–46]

$$x_A^{surf} = \int_0^{D/2} \left[x_A(z) - x_{A,coex}^{(1)} \right] dz, \quad D \to \infty. \tag{11}$$

If the wall is *nonwet* or *partially wet* (PW) [38–45], x_A^{surf} tends to a finite value ($x_{A,coex}^{surf}$) when $x_A \to x_{A,coex}^{(1)}$ from the one-phase region. On the other hand, for a *wet* or *completely wet* (CW) wall, $x_A^{surf} = \infty$—corresponding to an infinitely thick A-rich wetting layer coating the wall, separated from the B-rich bulk by a flat interface.

At the coexistence curve $x_{A,coex}^{(1)}$, the surface excess free energy is that of an A-rich phase ($F_{s,coex}^{B\text{-rich}}$) if the wall is PW. For a CW wall, we have $F_s = F_{S,coex}^{A\text{-rich}} + \sigma$. These quantities also determine the contact angle θ [cf. (1)] at which an AB interface in the PW region meets the wall [38–45]

$$\cos\theta = \frac{(F_{s,coex}^{B\text{-rich}} - F_{s,coex}^{A\text{-rich}})}{\sigma}, \quad \text{if } F_{s,coex}^{B\text{-rich}} - F_{s,coex}^{A\text{-rich}} < \sigma. \tag{12}$$

If we increase the temperature along the coexistence curve $x_{A,coex}^{(1)}$, one encounters a wetting transition at temperature T_w (Fig. 1), where the state of the wall changes from PW ($T < T_w$) to CW ($T > T_w$). This transition may be either *second order* [Fig. 1(a)] or *first order* [Fig. 1(b)]. In the second-order case, x_A^{surf} diverges continuously when $T \to T_w^-$. In the first-order case, there is a discontinuous jump in x_A^{surf} from a finite value at T_w^- to ∞ at T_w^+. In the latter case, there is also a *prewetting transition* in the one-phase region [Fig. 1(b)]. Here, the thickness of the A-rich surface layer jumps from a smaller value to a larger (but finite) value. This line of prewetting transitions ends in a prewetting critical point.

3.3 Lattice and Continuum Models for SDSD

A microscopic model for SDSD is obtained by associating Kawasaki spin-exchange kinetics [47] with the Ising Hamiltonian in (7). In Kawasaki kinetics, randomly-chosen neighboring spins are interchanged, keeping the overall composition of the mixture fixed.

Binder [48] has used the master equation for the Kawasaki-Ising model to derive evolution equations for the order parameter $\langle \sigma_i \rangle(t) = m(\vec{r}, t)$. These equations become analytically and numerically tractable in the mean-field (MF) approximation. Binder and Frisch [49] have extended this approach to the semi-infinite Kawasaki-Ising model with a short-ranged surface field confined to the surface layer, i.e., $V(z) = 0$ in (7). In this case, we denote the order parameter as $\langle \sigma_i \rangle(t) = m_n(\vec{\rho}, t)$, where the surface lies at $n = 0$. Then, $n = 1$ denotes the first layer of the Ising system; and $n \geq 2$ labels the inner layers. The MF dynamical model obtained by Binder and Frisch is as follows:

(i) $n \geq 3$ (bulk case)

$$\begin{aligned}
2\tau_s \frac{d}{dt} m_n(\vec{\rho}, t) = {} & -6m_n(\vec{\rho}, t) + m_{n-1}(\vec{\rho}, t) + m_{n+1}(\vec{\rho}, t) + \sum_{\Delta\vec{\rho}} m_n(\vec{\rho} + \Delta\vec{\rho}, t) \\
& + [1 - m_n(\vec{\rho}, t) m_{n-1}(\vec{\rho}, t)] \tanh\left\{ \frac{J}{k_B T} \left[m_{n+1}(\vec{\rho}, t) + m_{n-1}(\vec{\rho}, t) \right.\right. \\
& \left.\left. + \sum_{\Delta\vec{\rho}} m_n(\vec{\rho} + \Delta\vec{\rho}, t) - m_n(\vec{\rho}, t) - m_{n-2}(\vec{\rho}, t) - \sum_{\Delta\vec{\rho}} m_{n-1}(\vec{\rho} + \Delta\vec{\rho}, t) \right] \right\} \\
& + [1 - m_n(\vec{\rho}, t) m_{n+1}(\vec{\rho}, t)] \tanh\left\{ \frac{J}{k_B T} \left[m_{n+1}(\vec{\rho}, t) \right.\right. \\
& \left.\left. + m_{n-1}(\vec{\rho}, t) + \sum_{\Delta\vec{\rho}} m_n(\vec{\rho} + \Delta\vec{\rho}, t) - m_n(\vec{\rho}, t) \right] \right\}
\end{aligned}$$

$$- m_{n+2}(\vec{\rho},t) - \sum_{\Delta\vec{\rho}} m_{n+1}(\vec{\rho}+\Delta\vec{\rho},t)\Big]\Big\}$$

$$+ \sum_{\Delta\vec{\rho}} [1 - m_n(\vec{\rho},t) m_n(\vec{\rho}+\Delta\vec{\rho},t)] \tanh\Big\{\frac{J}{k_B T}\Big[m_{n+1}(\vec{\rho},t) + m_{n-1}(\vec{\rho},t)$$

$$+ \sum_{\Delta\vec{\rho}'} m_n(\vec{\rho}+\Delta\vec{\rho}',t) - m_{n+1}(\vec{\rho}+\Delta\vec{\rho},t)$$

$$- m_{n-1}(\vec{\rho}+\Delta\vec{\rho},t) - \sum_{\Delta\vec{\rho}'} m_n(\vec{\rho}+\Delta\vec{\rho}+\Delta\vec{\rho}',t)\Big]\Big\}. \tag{13}$$

Here, τ_s is the time-scale of spin-exchanges. In (13), exchanges of a spin at site $\vec{\rho}$ in layer n with spins in layers $n-1, n+1$, and the same layer n need to be considered. In the arguments of the tanh functions, the difference of the effective fields acting on the exchanged spins is found.

The kinetic equations near the wall are similar; one has to consider that a field H_1 is acting in layer 1, and that no spin exchange is possible into the layer $n = 0$ (the wall). Hence, for

(ii) $n = 2$

$$2\tau_s \frac{d}{dt} m_2(\vec{\rho},t) = -6m_2(\vec{\rho},t) + m_1(\vec{\rho},t) + m_3(\vec{\rho},t) + \sum_{\Delta\vec{\rho}} m_2(\vec{\rho}+\Delta\vec{\rho},t)$$

$$+ [1 - m_2(\vec{\rho},t) m_1(\vec{\rho},t)] \tanh\Big\{\frac{J}{k_B T}\Big[m_3(\vec{\rho},t) + m_1(\vec{\rho},t)$$

$$+ \sum_{\Delta\vec{\rho}} m_2(\vec{\rho}+\Delta\vec{\rho},t) - \frac{H_1}{J} - m_2(\vec{\rho},t) - \frac{J_s}{J}\sum_{\Delta\vec{\rho}} m_1(\vec{\rho}+\Delta\vec{\rho},t)\Big]\Big\}$$

$$+ [1 - m_2(\vec{\rho},t) m_3(\vec{\rho},t)] \tanh\Big\{\frac{J}{k_B T}\Big[m_3(\vec{\rho},t) + m_1(\vec{\rho},t)$$

$$+ \sum_{\Delta\vec{\rho}} m_2(\vec{\rho}+\Delta\vec{\rho},t) - m_4(\vec{\rho},t) - m_2(\vec{\rho},t) - \sum_{\Delta\vec{\rho}} m_3(\vec{\rho}+\Delta\vec{\rho},t)\Big]\Big\}$$

$$+ \sum_{\Delta\vec{\rho}} [1 - m_2(\vec{\rho},t) m_2(\vec{\rho}+\Delta\vec{\rho},t)]$$

$$\times \tanh\Big\{\frac{J}{k_B T}\Big[m_3(\vec{\rho},t) + m_1(\vec{\rho},t) + \sum_{\Delta\vec{\rho}} m_2(\vec{\rho}+\Delta\vec{\rho},t)$$

$$- m_3(\vec{\rho}+\Delta\vec{\rho},t) - m_1(\vec{\rho}+\Delta\vec{\rho},t)$$

$$- \sum_{\Delta\vec{\rho}'} m_2(\vec{\rho}+\Delta\vec{\rho}+\Delta\vec{\rho}',t)\Big]\Big\}. \tag{14}$$

Finally, for

(iii) $n = 1$ (now only 5 neighbors are available for an exchange)

$$
\begin{aligned}
2\tau_s \frac{d}{dt} m_1(\vec{\rho},t) = & -5m_1(\vec{\rho},t) + m_2(\vec{\rho},t) + \sum_{\Delta\vec{\rho}} m_1(\vec{\rho}+\Delta\vec{\rho},t) \\
& + [1 - m_1(\vec{\rho},t)m_2(\vec{\rho},t)] \tanh\left\{ \frac{J}{k_B T}\left[m_2(\vec{\rho},t) \right.\right. \\
& + \frac{H_1}{J} + \frac{J_s}{J} \sum_{\Delta\vec{\rho}} m_1(\vec{\rho}+\Delta\vec{\rho},t) \\
& \left.\left. - m_3(\vec{\rho},t) - m_1(\vec{\rho},t) - \sum_{\Delta\vec{\rho}} m_2(\vec{\rho}+\Delta\vec{\rho},t) \right]\right\} \\
& + \sum_{\Delta\vec{\rho}} [1 - m_1(\vec{\rho},t)m_1(\vec{\rho}+\Delta\vec{\rho},t)] \\
& \times \tanh\left\{ \frac{J}{k_B T}\left[m_2(\vec{\rho},t) + \frac{J_s}{J} \sum_{\Delta\vec{\rho}'} m_1(\vec{\rho}+\Delta\vec{\rho}',t) \right.\right. \\
& \left.\left. - m_2(\vec{\rho}+\Delta\vec{\rho},t) - \frac{J_s}{J} \sum_{\Delta\vec{\rho}'} m_1(\vec{\rho}+\Delta\vec{\rho}'+\Delta\vec{\rho},t) \right]\right\}. \qquad (15)
\end{aligned}
$$

Binder and Frisch [49] linearized the MF model in (13)–(15) to obtain a linear partial differential equation model, valid for $T > T_c$. They used this continuum model to study the kinetics of *surface enrichment*, i.e., the growth of surface layers for a stable binary mixture (at $T > T_c$), placed in contact with a wetting surface [50, 51].

In general, the continuum counterpart of the kinetic Ising model is expected to be more amenable to theoretical analysis. The first successful coarse-grained model for SDSD was proposed by Puri and Binder (PB) [52, 53], following earlier work by Ball and Essery [54]. The PB model can be obtained by suitable coarse-graining of (13)–(15). Here, we derive the PB model from general considerations. For phase separation driven by diffusion, the bulk order parameter obeys the Cahn-Hilliard-Cook (CHC) equation or *Model B* [55]:

$$
\begin{aligned}
\frac{\partial}{\partial t}\psi(\vec{r},t) &= -\vec{\nabla}\cdot\vec{J}(\vec{r},t) \\
&= \vec{\nabla}\cdot\left[D\vec{\nabla}\mu(\vec{r},t) + \vec{\theta}(\vec{r},t) \right] \\
&= \vec{\nabla}\cdot\left[D\vec{\nabla}\left(\frac{\delta\mathcal{F}}{\delta\psi} \right) + \vec{\theta}(\vec{r},t) \right]. \qquad (16)
\end{aligned}
$$

Here, $\vec{J}(\vec{r},t)$ is the current; D is the diffusion constant; and $\mu(\vec{r},t)$ is the local chemical potential difference between species A and B. The Gaussian white noise $\vec{\theta}(\vec{r},t)$ obeys the relations

$$
\begin{aligned}
\overline{\vec{\theta}(\vec{r},t)} &= 0, \\
\overline{\theta_i(\vec{r}',t')\theta_j(\vec{r}'',t'')} &= 2Dk_B T\delta_{ij}\delta(\vec{r}'-\vec{r}'')\delta(t'-t''),
\end{aligned} \qquad (17)
$$

where the bars denote an averaging over the noise ensemble.

Replacing the free-energy functional from (9) in (16), we obtain

$$\frac{\partial}{\partial t}\psi(\vec{r},t) = \vec{\nabla}\cdot\left\{D\vec{\nabla}\left[-k_B(T_c - T)\psi + \frac{k_B T}{3}\psi^3 - J\nabla^2\psi + V(z)\right] + \vec{\theta}\right\}, \quad z > 0. \tag{18}$$

This fourth-order partial differential equation must be supplemented by two boundary conditions wherever a surface is introduced. The boundary conditions are obtained as follows. At the surface, the order parameter is expected to relax rapidly to its equilibrium value and it can be treated as a non-conserved quantity. Therefore, we assume a relaxational (or *Model A* [55]) kinetics for the order parameter at the surface. This yields (ignoring thermal fluctuations) the boundary condition:

$$\begin{aligned}\tau\frac{\partial}{\partial t}\psi(\vec{\rho},0,t) &= -\frac{\delta\mathcal{F}}{\delta\psi(\vec{\rho},0,t)} \\ &= [(q-2)J_s + J - k_B T]\psi + H_1 + \frac{J}{2}\frac{\partial\psi}{\partial z}\bigg|_{z=0} \\ &\quad + J_s\nabla_{\parallel}^2\psi(\vec{\rho},0,t),\end{aligned} \tag{19}$$

where τ sets the time-scale. The second boundary condition is the no-flux or zero-current condition at $z = 0$:

$$0 = \left\{D\frac{\partial}{\partial z}\left[-k_B(T_c - T)\psi + \frac{k_B T}{3}\psi^3 - J\nabla^2\psi + V(z)\right] + \theta_z\right\}_{z=0}. \tag{20}$$

At first sight, the use of a nonconserved boundary condition (19), for a model with conserved order parameter may be surprising. However, these boundary conditions are justified provided that the bulk correlation length $\xi_b \gg a$ (with a the lattice spacing). This can be rationalized in the framework of the linearized theory, reported in Ref. [49].

Let us rescale the model in (18)–(20) (for $T < T_c$) into dimensionless units. We use the natural scales for the order parameter, space and time to introduce the following rescaled quantities:

$$\begin{aligned}\psi' &= \frac{\psi}{\psi_0}, \qquad \psi_0 = \sqrt{3\left(\frac{T_c}{T} - 1\right)}, \\ \vec{r}' &= \frac{\vec{r}}{\xi_b}, \qquad \xi_b = \left[\frac{q}{2}\left(1 - \frac{T}{T_c}\right)\right]^{-1/2}, \\ t' &= \frac{t}{t_0}, \qquad t_0 = \frac{\xi_b^2}{D k_B(T_c - T)}, \\ \vec{\theta}' &= \frac{t_0}{\xi_b\psi_0}\vec{\theta}, \\ V'(z') &= \frac{1}{\psi_0 k_B(T_c - T)}V(\xi_b z').\end{aligned} \tag{21}$$

Dropping the primes, we obtain the dimensionless CHC equation:

$$\frac{\partial}{\partial t}\psi(\vec{r},t) = \vec{\nabla}\cdot\left\{\vec{\nabla}\left[-\psi+\psi^3-\frac{1}{2}\nabla^2\psi+V(z)\right]+\vec{\theta}\right\}, \quad z>0, \tag{22}$$

where

$$\begin{aligned}\overline{\vec{\theta}(\vec{r},t)} &= 0,\\ \overline{\theta_i(\vec{r'},t')\theta_j(\vec{r''},t'')} &= 2\epsilon\delta_{ij}\delta(\vec{r'}-\vec{r''})\delta(t'-t'').\end{aligned} \tag{23}$$

The noise amplitude is

$$\epsilon = \frac{1}{3}\left(\frac{T_\mathrm{c}}{T}-1\right)^{-2}\xi_\mathrm{b}^{-d}. \tag{24}$$

The dimensionless boundary conditions are as follows:

$$\tau_0\frac{\partial}{\partial t}\psi(\vec{\rho},0,t) = h_1 + g\psi(\vec{\rho},0,t) + \gamma\left.\frac{\partial\psi}{\partial z}\right|_{z=0} + \tilde{\gamma}\nabla_\parallel^2\psi(\vec{\rho},0,t), \tag{25}$$

$$0 = \left\{\frac{\partial}{\partial z}\left[-\psi+\psi^3-\frac{1}{2}\nabla^2\psi+V(z)\right]+\theta_z\right\}_{z=0}, \tag{26}$$

where $\tau_0 = \tau D/\xi_\mathrm{b}^2$. The other parameters in the boundary conditions are

$$h_1 = \frac{H_1}{\psi_0 k_B(T_\mathrm{c}-T)}, \tag{27}$$

$$g = \frac{(q-2)J_\mathrm{s}+J-k_BT}{k_B(T_\mathrm{c}-T)}, \tag{28}$$

$$\gamma = \frac{J}{2\xi_\mathrm{b}k_B(T_\mathrm{c}-T)}, \tag{29}$$

$$\tilde{\gamma} = \frac{J_\mathrm{s}}{\xi_\mathrm{b}^2 k_B(T_\mathrm{c}-T)}. \tag{30}$$

Equation (25) rapidly relaxes $\psi(\vec{\rho},0,t)$ to its equilibrium value. If the equilibrium morphology is CW, we can drop the lateral diffusion term in (25) because the order parameter is uniform at the surface—in that case, we also set $\tau_0 = 0$. The surface potential and the parameters $h_1, g, \gamma, \tilde{\gamma}, \epsilon$ determine the equilibrium phase diagram of the surface [12, 13, 56, 57].

We finally note that the boundary conditions in (25), (26) have also been derived by Diehl and Janssen [38] from symmetry arguments as natural boundary conditions for Model B near criticality. These arguments do not make any connections to parameters of a microscopic lattice model, as done in (27)–(30). The model described above is appropriate for a semi-infinite geometry. The extension to a thin-film (or any other) geometry is straightforward—the boundary conditions in (19)–(20) have to be implemented on all surfaces with appropriate parameters. In Sect. 4, we will present results for SDSD in a thin film.

The modeling described above has been in the context of diffusive dynamics, which is appropriate for solid mixtures. However, many of the experiments on SDSD involve fluid

mixtures, where hydrodynamic effects play an important role in the intermediate and late stages of phase separation—as discussed in Sect. 2.2 [1–5]. Again, one could consider microscopic models, e.g., molecular dynamics (MD) simulations of mixtures near surfaces. On a coarse-grained level, the interplay between phase separation and hydrodynamic effects can be studied in the framework of *Model H* [55] at a surface. Model H consists of the coupled dynamics of the order-parameter field and the fluid velocity field (which obeys the Navier-Stokes equation). The boundary conditions on the order-parameter field are analogous to those described above. However, these must now be supplemented with boundary conditions on the velocity field, e.g., the velocity vanishes at the surface. There have been a number of experimental and theoretical studies of SDSD in fluid mixtures, and these have been reviewed by Tanaka [58] and Puri and Frisch [12, 13].

3.4 Interplay of Wetting and Phase Separation

Let us next discuss the kinetics of wetting-layer growth, and phase separation near the wetting layer, for a semi-infinite geometry. At present, we use the continuum model in (22)–(26). A comparison between lattice and continuum models will be presented in Sect. 3.5. We consider power-law potentials:

$$\begin{aligned} V(z) &= -V_0, \quad z \le 1, \\ &= -\frac{V_0}{z^n}, \quad z > 1. \end{aligned} \tag{31}$$

The lower cut-off in the potential is chosen to avoid the singularity at $z = 0$. Power-law potentials are common in the context of surface-molecule interactions, e.g., $n = \kappa - d$ with $\kappa = 6$ and 7 corresponds to cases with *non-retarded* and *retarded* van der Waals' interactions, respectively [59]. The short-ranged case is recovered in the limit $n \to \infty$. The dimensionless surface field is $h_1 = -V(0) = V_0$.

In Fig. 3, we show snapshots (frames on left) of a segregating binary mixture in $d = 2$ with average order parameter ψ_0. The case with $\psi_0 = 0$ [see Fig. 3(a)] corresponds to a mixture with 50% A and 50% B, i.e., a critical quench. The simulation details are provided in the figure caption. The surface at $z = 0$ is completely wetted by the component A (marked in black), and shows a multi-layered morphology, i.e., wetting layer followed by depletion layer, etc. This morphology is time-dependent and propagates into the bulk, as seen from the laterally averaged profiles $\psi_{\rm av}(z, t)$ vs. z (frames on right). These are obtained by averaging $\psi(x, z, t)$ along the x-direction for a typical evolution, and further averaging over 200 independent runs. (This procedure is the numerical counterpart of the lateral-averaging which yielded the density-depth profiles in Fig. 2.) The averaging procedure gives $\psi_{\rm av}(z, t) \simeq \psi_0$ in the bulk, where the phase-separation profiles are randomly oriented. The wetting profiles are characterized by the zero-crossings of $\psi_{\rm av}(z, t) - \psi_0$, and $R_1(t)$ and $R_2(t)$ denote the first and second zeros, respectively.

Figure 3(b) shows the evolution for an off-critical quench with $\psi_0 = -0.4$, corresponding to a mixture with 30% A (the preferred component) and 70% B. Notice that the bulk (large z) is characterized by a droplet morphology, which is standard for phase separation in an off-critical system [60–63]. As in Fig. 3(a), there is a wetting layer of the preferred component at the surface, followed by a depletion layer. At comparable times, the thickness of the wetting and depletion layers is larger than in the case with $\psi_0 = 0$.

Figure 3(c) shows SDSD in an extremely off-critical mixture, with $\psi_0 = -0.8$ or 10% A and 90% B. In this case, the thermal fluctuations are not sufficient to nucleate an A-rich

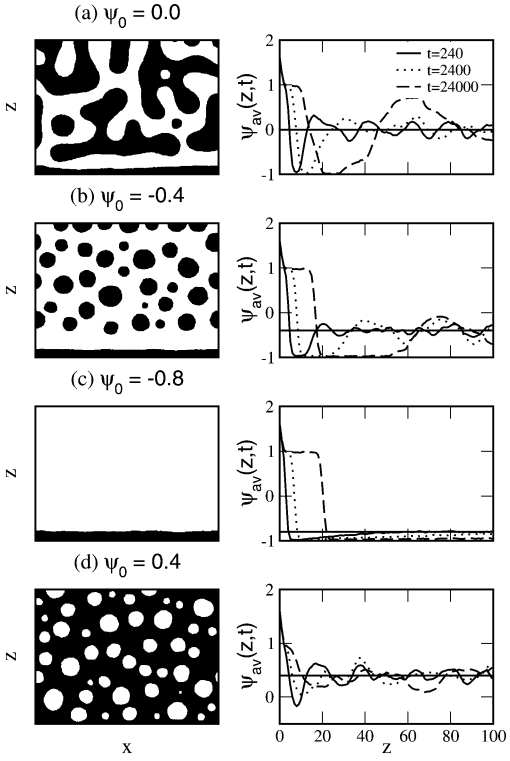

Fig. 3 SDSD in an unstable AB mixture, evolving from a disordered initial condition. This consists of random fluctuations about an average order parameter ψ_0. The snapshots (frames on the left) are obtained from an Euler-discretized version of (22)–(26) on a $d = 2$ square lattice of size $L_x \times L_z$ (with $L_x = 400$ and $L_z = 300$). The mesh sizes in space and time are $\Delta x = 1$ and $\Delta t = 0.03$. Periodic boundary conditions are applied at $x = 0, L_x$; and flat boundary conditions are applied at $z = L_z$. The surface is located at $z = 0$ and attracts A ($\psi > 0$, marked in *black*) through a power-law potential with $n = 4$ and $V_0 = h_1 = 0.8$. The other parameter values are $g = -0.4$ and $\gamma = 0.4$, corresponding to complete wetting in equilibrium. The noise amplitude is $\epsilon = 0.041$, which corresponds to a deep quench with $T \simeq 0.22 T_c$ from (24). The frames on the right show the corresponding laterally averaged profiles at dimensionless times $t = 240, 2400, 24000$. A *solid line* is drawn at $\psi_{av} = \psi_0$, the average value of the order parameter. Notice the two-step wetting profile at the surface

droplet on the time-scale of the simulation. Thus, there is no bulk phase separation, but there is still a rapid growth of the surface wetting layer. However, the behavior is qualitatively different from that for $\psi_0 = 0, -0.4$, due to the absence of bulk phase separation. The corresponding depth profiles show that the A-rich wetting layer is followed by a thick layer which is moderately depleted in A.

Figure 3(d) shows the evolution for the case with $\psi_0 = 0.4$, i.e., 70% A and 30% B. We will discuss this case shortly, but let us first discuss the evolution of the wetting profiles in Figs. 3(a)–(b), where the bulk undergoes phase separation. The depletion-layer thickness is $h(t) = R_2(t) - R_1(t)$. The growth of the wetting layer is driven by two factors:

(1) The gradient of the surface potential drives A to the wetting layer with a current $-V'(R_1)$.

(2) The chemical potential is higher on the curved surface of bulk A-rich domains (of size L) than on the flat wetting layer (of size ∞). This difference is estimated as σ/L, and the corresponding current at the wetting layer is $-\sigma/(Lh)$.

Thus the A-current in the z-direction is obtained as

$$J_z \simeq -V'(R_1) - \frac{\sigma}{Lh}. \tag{32}$$

To estimate $h(t)$, we assume that the wetting and depletion layers have an overall composition of ψ_0 [64, 65]. Then

$$R_2(t) \simeq \frac{2}{1+\psi_0} R_1(t), \qquad h(t) \simeq \frac{1-\psi_0}{1+\psi_0} R_1(t). \tag{33}$$

Using the power-law potential in (31), and $h(t)$ from (33), (32) yields [64, 65]

$$\frac{dR_1}{dt} = -J_z \simeq \frac{nh_1}{{R_1}^{n+1}} + \frac{\sigma}{LR_1}\left(\frac{1+\psi_0}{1-\psi_0}\right). \tag{34}$$

The bulk length scale obeys the LS growth law $L(t) = f(\psi_0)(\sigma t)^{1/3}$, where the function $f(\psi_0)$ is known analytically for $|\psi_0| \to 1$ [1], but only numerically for other values of ψ_0 [60–62]. For $n > 1$, the first term on the RHS of (34) is dominant at early times, and the second term is dominant at late times. Then, the growth regimes are

$$\begin{aligned} R_1(t) &\sim (h_1 t)^{1/(n+2)}, \quad t \ll t_c, \\ &\sim \sqrt{\frac{(1+\psi_0)}{f(\psi_0)(1-\psi_0)}}(\sigma t)^{1/3}, \quad t \gg t_c. \end{aligned} \tag{35}$$

The crossover time t_c is estimated by matching the early-time and late-time length scales as (for $n > 1$)

$$t_c \sim h_1^{3/(n-1)} \sigma^{-(n+2)/(n-1)} \left[\frac{f(\psi_0)(1-\psi_0)}{(1+\psi_0)}\right]^{3(n+2)/[2(n-1)]}. \tag{36}$$

The crossover between the potential-dependent regime and the universal LS regime ($R_1 \sim t^{1/3}$) can be extremely delayed, depending on the system parameters and mixture composition. This explains the diverse growth exponents reported by various experiments and numerical simulations [12, 13]. Figure 4(a) plots $\ln[R_1(t)]$ vs. $\ln t$ for $\psi_0 = 0, -0.2, -0.4, -0.6$ and illustrates this crossover behavior.

Let us briefly remark on two other cases: (a) the power-law potential with $n = 1$, and (b) the short-ranged potential $V(z) = -V_0 \exp(-z/z_0)$. For $V(z) \sim -z^{-1}$, both terms on the RHS of (34) are comparable resulting in the LS growth law, $R_1(t) \sim t^{1/3}$. On the other hand, the short-ranged potential yields a logarithmic early-time growth, $R_1(t) \sim z_0 \ln(h_1 t/z_0^2)$, which rapidly crosses over to the LS law.

Next, consider very off-critical quenches ($\psi_0 \ll 0$), where there is no bulk phase separation [see Fig. 3(c)]. In this case, there are no bulk droplets which feed the wetting layer. Thus, the chemical potential in the bulk is the uniform value $\mu_0 \simeq {\psi_0}^3 - \psi_0$. The current to the wetting layer is $-\mu_0/h$, where $h(t)$ is the scale on which the order parameter exponentially saturates to its bulk value [see the depth profiles in Fig. 3(c)]. We assume a simple

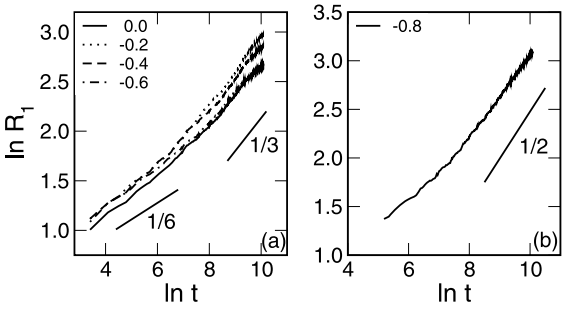

Fig. 4 (**a**) Plot of ln R_1 vs. ln t for mixtures with $\psi_0 = 0, -0.2, -0.4, -0.6$. The simulation details are provided in the caption of Fig. 3. The straight lines have slopes 1/6 and 1/3, respectively. The exponent $\phi = 1/6$ arises for potential-dependent growth in the case of non-retarded van der Waals' interactions with $n = 4$ in $d = 2$ [see (35)]. (**b**) Plot of ln R_1 vs. ln t for an extremely off-critical mixture with $\psi_0 = -0.8$. The *straight line* has a slope of 1/2, corresponding to diffusive growth

form for $\psi(z,t)$ as follows [64, 65]:

$$\begin{aligned} \psi(z,t) &\simeq 1, \quad z < R_1(t), \\ &\simeq \psi_0 - B_0 e^{-(z-R_1)/h}, \quad z > R_1(t), \end{aligned} \tag{37}$$

where B_0 is a parameter. The composition constraint yields

$$h(t) \simeq \frac{(1-\psi_0)}{B_0} R_1(t). \tag{38}$$

Then, (34) becomes

$$\begin{aligned} \frac{dR_1}{dt} &\simeq \frac{nh_1}{{R_1}^{n+1}} + \frac{\mu_0 B_0}{1-\psi_0}\frac{1}{R_1} \\ &= \frac{nh_1}{{R_1}^{n+1}} + \frac{|\psi_0|(1+\psi_0)B_0}{R_1}. \end{aligned} \tag{39}$$

The corresponding growth regimes in this case are (for any value of n)

$$\begin{aligned} R_1(t) &\sim (h_1 t)^{1/(n+2)}, \quad t \ll t_c, \\ &\sim \left[|\psi_0|(1+\psi_0)B_0\right]^{1/2} t^{1/2}, \quad t \gg t_c. \end{aligned} \tag{40}$$

The crossover from a potential-dependent growth law to a universal diffusive growth law occurs at

$$t_c \sim h_1^{2/n} \left[|\psi_0|(1+\psi_0)B_0\right]^{-(n+2)/n}. \tag{41}$$

In Fig. 4(b), we plot ln$[R_1(t)]$ vs. ln t for $\psi_0 = -0.8$, showing the diffusive growth of the wetting layer. For a short-ranged surface potential, the initial growth regime is logarithmic, as before.

Finally, we consider off-critical compositions with $\psi_0 > 0$, so that the majority component wets the surface. Figure 3(d) shows a snapshot for the case with $\psi_0 = 0.4$—now the droplets are of the non-wetting component. A thin wetting layer is formed which barely

grows, as seen in Fig. 3(d). This is because the bulk droplets now compete with (rather than feed) the wetting layer, as the chemical potential for A is lower on the surface of the drops. Thus, only the first term on the RHS of (34) is relevant, which gives $R_1(t) \sim t^{1/(n+2)}$. Actually, the wetting-layer growth is even slower because the chemical-potential gradient actually drives A into the bulk. Similar considerations apply for other values of $\psi_0 > 0$, when the bulk undergoes phase separation.

The extremely off-critical case (with $\psi_0 \gg 0$) is similar to enrichment kinetics seen for $T > T_c$ [50, 51], provided no droplets are nucleated. If droplets are nucleated, the scenario described for $\psi_0 = 0.4$ applies again.

The discussion so far has followed the work of Puri, Binder et al. [52, 53, 64–66]. Let us briefly discuss other important theoretical studies of this problem. Brown and Chakrabarti [67] undertook a Langevin simulation of SDSD in $d = 2$ with both short-ranged and long-ranged surface potentials. Their model was similar to the PB model described in Sect. 3.3, but the parameter values correspond to a PW surface morphology. Brown and Chakrabarti found that the wetting layer obeyed the LS growth law, $R_1(t) \sim t^{1/3}$.

A comprehensive *cell dynamical system* [60–62] study of SDSD in $d = 2, 3$ was reported by Marko [68], who studied cases with both short-ranged and long-ranged surface potentials. Marko studied domain morphologies and the laterally averaged profiles in both PW and CW cases. For the PW morphology, he found results consistent with those of Brown and Chakrabarti [67]. In the CW case, he found a drastic slowing down of wetting layer growth, which is consistent with the potential-dependent growth regime in (35).

There have also been Langevin simulations of SDSD on patterned substrates by Karim et al. [69], in conjunction with experiments on polymer blends. These studies suggested ways of controlling the phase-separation morphology near the surface. Lee et al. [70] have also adapted the PB model described in Sect. 3.3 to study the effect of fixed obstacles with non-rectangular shapes (e.g., spheres or cylinders) on spinodal decomposition. In recent work, Jaiswal and Puri [71] have studied SDSD at both *chemically patterned* and *physically patterned* surfaces. They focused upon the interplay between the pattern length scale (which is fixed) and the divergent length scales of wetting and phase separation.

Finally, Yan et al. [72, 73] have studied the formation of lamellar structures in two-step SDSD in polymer blends. For polymer mixtures, various authors including Yan et al. have used the Flory-Huggins-de Gennes free energy (rather than the ψ^4 free energy) to model phase separation. Yan et al. study SDSD subsequent to two-step quenches in both critical and off-critical mixtures.

3.5 Comparison of Lattice and Continuum Models

In (13)–(15), we have presented MF dynamical equations for the Kawasaki-Ising model as a lattice analog of Model B amended by free surfaces. The stationary solutions of these equations correspond to the inhomogeneous molecular-field equations in equilibrium [49]:

$$m_n(\vec{\rho}) = \tanh\left[\frac{H_n^{\text{eff}}(\vec{\rho})}{k_B T}\right], \quad n = 1, 2, \ldots. \tag{42}$$

Here $H_n^{\text{eff}}(\vec{\rho})$ is the "effective field" acting on the spin in layer n and site $\vec{\rho}$ in this layer:

$$H_n^{\text{eff}}(\vec{\rho}) = J\left[m_{n+1}(\vec{\rho}) + m_{n-1}(\vec{\rho}) + \sum_{\Delta\vec{\rho}} m_n(\vec{\rho} + \Delta\vec{\rho})\right] + H, \quad n \geq 2. \tag{43}$$

For the surface layer ($n = 1$), one has an analogous equation, but $H_1^{\rm eff}(\vec{\rho})$ now accounts for the missing neighbor (no spin exists for $n = 0$); the surface magnetic field H_1; and the change of interactions ($J_s \neq J$) in the surface layer:

$$H_1^{\rm eff}(\vec{\rho}) = J m_2(\vec{\rho}) + J_s \sum_{\Delta\vec{\rho}} m_1(\vec{\rho} + \Delta\vec{\rho}) + H + H_1. \tag{44}$$

It is also straightforward to obtain the associated free energy, which can be decomposed into layer energies $E(n)$ and layer entropies $S(n)$ [49, 74]

$$F = \sum_n [E(n) - T S(n)]. \tag{45}$$

Here, $\sum_n E(n)$ is found from (7) by replacing σ_i by its average $\langle \sigma_i \rangle = m_n(\vec{\rho})$ in the Hamiltonian. The entropy $S(n)$ can be rewritten in terms of the familiar entropy of mixing:

$$\frac{S(n)}{k_B T} = \sum_{\vec{\rho}} \left\{ \frac{1 + m_n(\vec{\rho})}{2} \ln \left[\frac{1 + m_n(\vec{\rho})}{2} \right] + \frac{1 - m_n(\vec{\rho})}{2} \ln \left[\frac{1 - m_n(\vec{\rho})}{2} \right] \right\}. \tag{46}$$

Equations (42)–(44) can also be derived by minimizing the free energy, considering it as a functional of the local magnetizations, $\delta F / \delta m_n(\vec{\rho})|_{T,H,H_1} = 0$. The free energy in (9) is just the continuum approximation to (45).

This lattice theory is quantitatively equivalent to the continuum approximation only if the bulk correlation length ξ_b is much larger than the lattice spacing a. This consideration carries over to the dynamics: Equations (18)–(20) in the absence of noise ($\epsilon = 0$) are equivalent to (13)–(15) if $\xi_b \gg a$ [49, 74]. Of course, molecular field theory for a nearest neighbor Ising model, as described by (13)–(15) and (42)–(46) can be only accurate if one is not considering the vicinity of the bulk critical temperature T_c.

In view of this situation, two ways out of this problem are conceivable. We could consider (22)–(26) as a phenomenological model, treating the strength ϵ of thermal noise in (23) as a variable parameter. Then, we treat the constants $h_1, g, \gamma, \tilde{\gamma}$ as free parameters of the problem, rather than giving them the values resulting from the Ising model Hamiltonian. Since the boundary condition in (25), resulting from the surface free energy term $\int dz \delta(z) \mathcal{F}_s\{\psi(\vec{\rho}, z)\}$, contains a delta function under the integral in (9), particular care is needed for the numerical treatment of this boundary condition. The discretization of (22) can lead to inconsistent results, if one disregards the conditions for which (25) was derived. This point has been emphasized by Henderson and Clarke [75, 76] and Fukuda et al. [75, 76]. These authors consider alternative methods of setting up the boundary conditions in the Ginzburg-Landau (GL) model. These approaches capture the early-time dynamics accurately, but would give similar results to ours at late times and divergent length scales.

Given the fact that fluctuations are irrelevant in the late stages of coarsening [1], one can alternatively resort to the direct numerical solution of (13)–(15). In some cases, this is more convenient than approximating this set of discrete equations by a continuum theory, which is again discretized on a lattice for numerical solution. Of course, if we worked in the regime very close to T_c where $\xi_b \gg a$, the continuum approach may save numerical effort, since the extreme choice for the spatial discretization length Δx is $\Delta x \simeq \xi_b$ [52, 53]. Then, the number of grid points of the discretized continuum model is much smaller than the number of lattice points of the original lattice model, considering the same volume. However, as argued above, for the present problem we are not really interested in the vicinity of T_c, and if $\xi_b \simeq a$, the direct numerical solution of (13)–(15) does not require more effort than a solution

based on the CHC equation (22) [74]. The advantage of (13)–(15) is that the conservation law for the concentration is treated exactly in all layers, and there is no ambiguity about the physical meaning of the parameters (J, J_s, H_1) of the model [74, 77].

At the end of this section, we emphasize that it is also of interest to directly simulate the full Kawasaki-Ising model with Monte Carlo methods. Unlike (13)–(15), then thermal fluctuation effects would be fully included, and such a treatment would be preferable to describe the initial stages of phase separation correctly, even though the numerical effort is much larger than what is needed to solve (13)–(15). Since Monte Carlo studies have proven to be most valuable for bulk Ising systems without surface effects to clarify the behavior of spinodal decomposition from the early to the late stages [78–80], recently Majumder and Das [81] have undertaken such study of the model in (7).

Another useful extension concerns a proper description of the processes on the atomistic scale. Equations (13)–(15) are based on a direct exchange A $\leftrightarrow$ B of particles at nearest neighbor sites [47]. However, in real solid binary alloys such a direct exchange of atoms does not occur, rather one expects vacancy-mediated exchange. Thus, there is a small fraction of vacant sites on the lattice, and A or B particles can jump to nearest (or next nearest) vacant sites only. Monte Carlo simulations have shown that spinodal decomposition effected by this vacancy mechanism is qualitatively very similar to spinodal decomposition based on the direct exchange mechanism [82]. The local molecular-field approach as described by (13) has also been generalized to this more realistic, vacancy-mediated phase separation [83–85]. Since such models have not yet extended to treat the effect of surfaces, we shall not consider them further here. Of course, at the coarse-grained continuum level of description (16), such microscopic details do not make a difference.

4 Phase Separation in a Confined Geometry

Next, let us focus on the kinetics of phase separation in a confined geometry. As stated earlier, the modeling of phase separation in confined geometries is a straightforward generalization of the semi-infinite case [86]. The phase-separation dynamics of confined mixtures is more complex due to the interaction of SDSD waves originating from different surfaces. Inspite of the rich phenomenology, there have been relatively few theoretical investigations of these problems [86–90], though there continue to be many experimental studies [91].

4.1 Equilibrium Morphologies in Thin Films

In Sect. 3.2, we gave a brief review of wetting phenomena at surfaces. This provides the basis to understand the equilibrium behavior of binary mixtures in thin films [92–102]. If the walls are neutral (i.e., they have the same attractive interactions with both A and B), the critical concentration remains $x_A^{crit} = 1/2$. However, the critical temperature $T_c(D)$ is lowered [92, 93, 98, 99] relative to the bulk:

$$T_c - T_c(D) \propto D^{-1/\nu}, \tag{47}$$

where $\nu \simeq 0.629$ [103, 104] is the critical exponent of the correlation length ξ_b of concentration fluctuations (in the universality class of the $d = 3$ Ising model). Clearly, critical correlations at finite D can become arbitrarily large only in the lateral direction parallel to the film. Thus, the transition at $T_c(D)$ belongs to the class of the $d = 2$ Ising model. The states below the coexistence curve of the thin film correspond to two-phase equilibria characterized by lateral phase separation.

When there is a preferential attraction of A to the walls, the phase diagram of the thin film is no longer symmetric with respect to $x_A = 1/2$. The shift of x_A^{crit} and the resulting change of the coexistence curve, is the analog of *capillary condensation of gases* [96, 105] for binary mixtures.

The coexisting phases in the region below the coexistence curve of the thin film are inhomogeneous in the direction perpendicular to the walls [see Fig. 1(c)]. In the A-rich phase, we expect only a slight enhancement of the order parameter $\psi(z)$, which is defined in terms of the densities $n_A(z)$, $n_B(z)$ as

$$\psi(z) = \frac{n_A(z) - n_B(z)}{n_A(z) + n_B(z)}. \tag{48}$$

In the B-rich phase, we expect pronounced enrichment layers. As $D \to \infty$, their thickness diverges for $T > T_w$ but stays finite for $T < T_w$. In a film of finite thickness, the width of A-rich surface layers also stays finite, e.g., for $T > T_w$, $x_A^{surf} \propto \ln D$ for short-range surface forces, while $x_A^{surf} \propto D^{1/3}$ for non-retarded van der Waals' forces [98, 106]. Thus, the wetting transition is always rounded off in a thin film. The prewetting line [Fig. 1(b)] does have an analog in films of finite thickness D, for sufficiently large D. This transition splits into a two-phase region at small x_A, between the thin-film triple point and the thin-film critical point on the B-rich side. This two-phase region corresponds to a coexistence between B-rich phases with A-rich surface layers, both of which have finite (but different) thickness. As $D \to \infty$, the thin-film critical point on the B-rich side moves into the prewetting critical point, while the thin-film triple point merges with the first-order wetting transition. On the other hand, when D becomes small, the thin-film critical point and the thin-film triple point may merge and annihilate each other. For still smaller D, the thin-film phase diagram has the shape shown in Fig. 1(a), although one has first-order wetting in the semi-infinite bulk [Fig. 1(b)].

Finally, we comment on the state encountered below the bulk coexistence curve, but above the coexistence curve of the thin film. When one crosses the bulk coexistence curve, there is a *rounded transition* towards a layered (stratified) structure with two A-rich layers at the walls and a B-rich layer in the middle. The temperature range over which this rounded transition is smeared is also of order $\Delta T \propto D^{-1/\nu}$ around T_c. Hence, for large D, this segregation in the direction normal to the walls may easily be mistaken (in experiments or simulations) as a true (sharp) phase transition. We stress that this is not a true transition—one is still in the one-phase region of the thin film, although the structure is strongly inhomogeneous! The situation qualitatively looks like the concentration profile shown in the upper part of Fig. 1(c). The difference is that, for $D \to \infty$, the thickness of true wetting layers scales sub-linearly with D, as noted above. However, for phase separation in the normal direction which gradually sets in when one crosses the bulk coexistence curve, one simply has A-rich domains of macroscopic dimensions (proportional to D) adjacent to both walls. Unfortunately, the layers resulting in this stratified structure are often referred to as "wetting layers" in the literature, although this is completely misleading. We reiterate that A-rich wetting layers only form when a B-rich domain extends to the surface, which is not the case here.

We also caution the reader that a picture in terms of A-rich layers at the walls and a B-rich domain in the inside of the film is an over-simplification because the thickness of the domain walls cannot really be neglected in the region $T_c(D) < T < T_c$, where a stratified structure occurs in equilibrium. This is seen from the relation $\xi_b \propto (1 - T/T_c)^{-\nu}$, in conjunction with (47), which shows that $\xi_b \sim O(D)$ at $T_c(D)$. Thus, domains and domain walls are not well-distinguished in the region under consideration, since the interfacial width is $O(\xi_b)$ [45, 46].

When the interface between A-rich and B-rich domains is treated as a sharp kink (this approximation is popular in theoretical treatments of wetting [38–45]), one might think that a sharp wetting transition could still be described in terms of the vanishing of the contact angle θ as $T \to T_w^-$ [Fig. 1(c)]. However, it is clear that for a correct treatment the finite width of the interface needs to be taken into account. Thus, for finite D, the contact angle in Fig. 1(c) is ill-defined, and the transition between the two states depicted in Fig. 1(c) is smooth, because a B-rich nonwet domain may also have a thin A-rich layer at its surface (x_A^{surf}, in general, is nonzero). One should also note that the contact "line" is distorted by line tension effects when it hits the wall, and the line tension of the interface at the wall would also modify (12) [107–110]. The difficulty of estimating the contact angle in finite geometries is well-known from studies of nanoscopic droplets [111–114].

The central conclusion in this subsection is that in the final equilibrium to which, for times $t \to \infty$ and for small D, the thin film evolves, there is no fundamental difference whether or not we are above or below the wetting transition temperature, but it matters whether $T < T_c(D)$ or $T > T_c(D)$.

4.2 SDSD in Thin Films

In recent work, Das et al. have undertaken Langevin [115] and MD [116, 117] studies of phase separation of AB mixtures in thin films with two parallel surfaces at $z = 0, D$. Experimental interest in this problem has focused on two cases:

(a) *symmetric films*, where the walls attract the same component of the mixture; and
(b) *antisymmetric films*, where the walls attract different components.

Here, we will focus on the case of symmetric films with identical surfaces. For this case, an appropriate potential is

$$V(z) = -V_0 \left[\frac{1}{(z+1)^n} + \frac{1}{(D+1-z)^n} \right]. \tag{49}$$

Here, we have removed the power-law singularity at $z = 0, D$ by assuming that the potential originates behind the surfaces.

In this subsection, we focus on continuum and molecular-field models of phase separation in thin films. The appropriate continuum model consists of (22), (25)–(26) in conjunction with the boundary conditions at $z = D$. For completeness, we present these boundary conditions here:

$$\tau_0 \frac{\partial}{\partial t} \psi(\vec{\rho}, D, t) = h_1 + g\psi(\vec{\rho}, D, t) - \gamma \left. \frac{\partial \psi}{\partial z} \right|_{z=D} + \tilde{\gamma} \nabla_{\|}^2 \psi(\vec{\rho}, D, t), \tag{50}$$

$$0 = \left\{ \frac{\partial}{\partial z} \left[-\psi + \psi^3 - \frac{1}{2} \nabla^2 \psi + V(z) \right] + \theta_z \right\}_{z=D}. \tag{51}$$

We use this model to study SDSD in a film with the power-law potential in (49) with $n = 3$. In Fig. 5, we show evolution snapshots and (xz)-cross-sections for films with $D = 5$ (frames on left) and $D = 10$ (frames on right). We consider the case of a critical quench with $\psi_0 = 0$. The potentials were chosen with $V_0 = 0.325$ for $D = 5$ and $V_0 = 0.11$ for $D = 10$, which correspond to the PW state in equilibrium. (Though there is no sharp wetting transition in the thin film, we use the terms *partially wet* or PW and *completely wet* or CW in analogy with the semi-infinite system.) A metastable layered structure forms at early times,

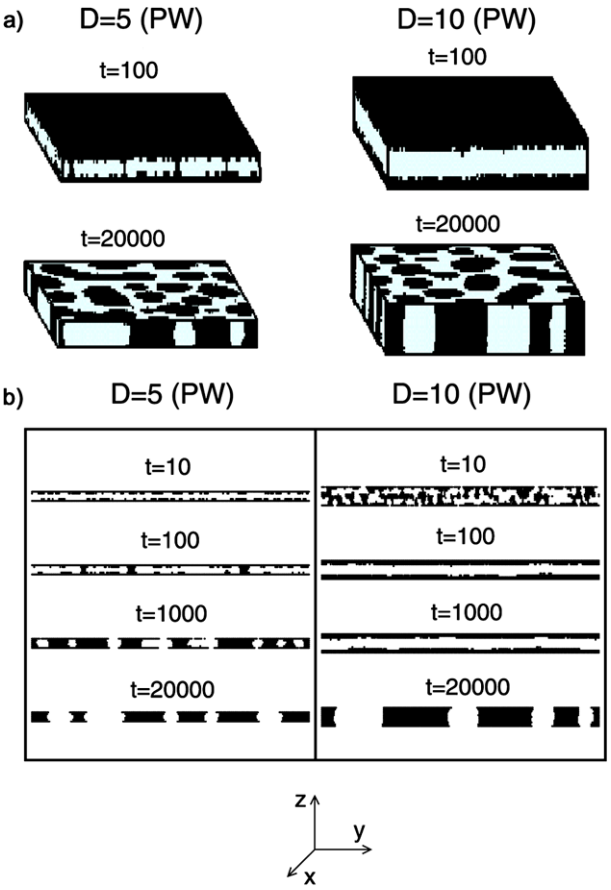

Fig. 5 SDSD in a symmetric thin film. These results were obtained from an Euler-discretized version of (22)–(23) on a lattice of size $L^2 \times D$ with $L = 256$. The discretization mesh sizes were $\Delta x = 1.0$ and $\Delta t = 0.02$. The boundary conditions in (25)–(26) (with $\tau_0 = 0$) were implemented at $z = 0$, D. Periodic boundary conditions were imposed in the x- and y-directions. The parameter values were $g = -0.4$ and $\gamma = 0.4$. The surface potential was of the form in (49) with $n = 3$, and $V_0 = 0.325$ (for $D = 5$) and $V_0 = 0.11$ (for $D = 10$). The noise amplitude was $\epsilon = 0.327$, which corresponds to a quench with $T \simeq 0.38 T_c$ from (24). These parameter values correspond to a PW equilibrium morphology. (**a**) Evolution snapshots for a critical binary mixture with $D = 5$ (frames on left) and $D = 10$ (frames on right). The A-rich regions ($\psi > 0$) are marked *black*, and the B-rich regions ($\psi < 0$) are unmarked. (**b**) Perpendicular cross-sections of the snapshots in (**a**) at $y = L/2$ in the (xz)-plane

since the kinetics of surface enrichment [50, 51] is much faster than the kinetics of phase separation. This layered structure is broken by spinodal fluctuations on longer time-scales, and the system forms domains which coarsen in directions parallel to the surface. We stress that the layered state can be very long-lived, and may be misinterpreted as evidence for the formation of wetting layers in experiments.

As before, laterally averaged profiles are obtained by averaging $\psi(x, y, z, t)$ along the x- and y-directions, and then further averaging over 5 independent runs. In Fig. 6, we show the depth profiles corresponding to the evolution for the $D = 10$ case in Fig. 5. The profile at time $t = 10$ shows the formation of two symmetric SDSD waves, which propagate towards the center of the film. The $t = 100$ profile shows the metastable layered state that has originated from these waves [see Fig. 5(a)]. This structure persists till $t \simeq 1000$. Finally, spinodal fluctuations break this structure and the averaged profile at $t = 20000$ is almost flat. Since a weak surface field amplitude ($V_0 = 0.11$) was chosen in this case, there is only a slightly A-rich region [$\psi_{av}(z, t) > 0$] near the walls and, therefore, only a slightly A-poor region [$\psi_{av}(z, t) < 0$] at the center.

It is also interesting to study (xy)-cross-sections of the evolution snapshots in Fig. 5. In Fig. 7, we show the cross-sections at $z = 5$ for $D = 10$. For early times ($t = 100$) the central region is strongly depleted in A due to the formation of the layered structure. The resultant morphology corresponds to a highly off-critical composition with droplets of A in a matrix

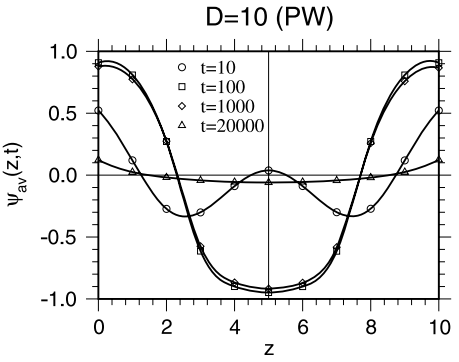

Fig. 6 Laterally averaged profiles for the evolution of the $D = 10$ film depicted in Fig. 5. We show profiles at the dimensionless times $t = 10, 100, 1000, 20000$

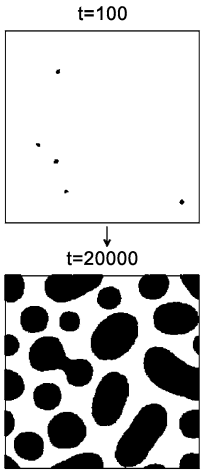

Fig. 7 Cross-sections of the snapshots for the $D = 10$ film in Fig. 5(a). The cross-sections are taken parallel to the surfaces at $z = 5$

of B. At later times ($t = 20000$), the central region has almost equal amounts of A and B. However, there is still a small depletion in A (see Fig. 6), and hence the growth morphology still contains droplets of A.

Let us next focus on the layer-wise correlation function, which is defined as [86]

$$C_{\parallel}(\vec{\rho}, z, t) = L^{-2} \int d\vec{\sigma}\ [\langle \psi(\vec{\sigma}, z, t)\psi(\vec{\sigma} + \vec{\rho}, z, t)\rangle - \langle \psi(\vec{\sigma}, z, t)\rangle\langle \psi(\vec{\sigma} + \vec{\rho}, z, t)\rangle], \quad (52)$$

where the angular brackets denote an averaging over independent runs. As the system is isotropic in the (xy)-plane, $C_{\parallel}$ does not depend on the direction of $\vec{\rho}$. The z-dependent lateral length scale $L_{\parallel}(z, t) \equiv L(z, t)$ is defined as $C_{\parallel}(\rho = L, z, t) = C_{\parallel}(0, z, t)/2$. For convenience, we denote $C_{\parallel}(\rho, z, t)$ as $C(\rho, t)$ in the following discussion. In Fig. 8, we plot the scaled correlation functions $C(\rho, t)/C(0, t)$ vs. ρ/L for $D = 10$. Notice that these correlation functions do not exhibit dynamical scaling as they correspond to qualitatively different morphologies (see Fig. 5). Thus, for $t = 1000$, the layered structure has not yet broken up, while lateral phase separation has occurred by $t = 20000$. Of course, dynamical scaling is recovered subsequent to the formation of well-formed laterally segregated domains ($t \geq 10000$ in this case).

We have also studied the time-dependence of the lateral domain size for the films with $D = 5, 10$ [115]. While the asymptotic growth is consistent with the expected LS growth law

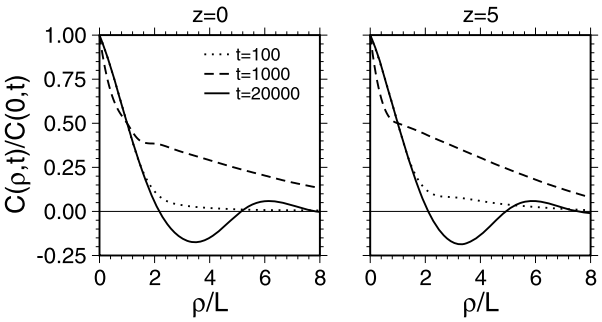

Fig. 8 Layer-wise correlation functions for the $D = 10$ evolution depicted in Fig. 5. We plot data for $C(\rho, t)/C(0, t)$ vs. ρ/L for $z = 0$ (wall) and $z = 5$ (center) at $t = 100, 1000, 20000$. The layer-wise length-scale $L(z, t)$ is defined as the distance over which $C(\rho, t)$ has decayed to 1/2 its maximum value (which arises at $\rho = 0$)

$L(t) \sim t^{1/3}$, which describes bulk domain growth, the early-time dynamics is complicated. The early-time data corresponds to the growth of bulk-like domains before the layered structure has formed. The spinodal fluctuations originate in the central region ($z \simeq D/2$) where the surface field is not felt, and propagate to the surface ($z = 0$). The break-up of the layered structure is characterized by the non-monotonic behavior of $L(z, t)$ vs. t.

Next, we consider the case where the surfaces have a CW morphology in equilibrium. In Fig. 9, we show evolution snapshots and (xz)-cross-sections for the CW case. The corresponding potential strengths were $V_0 = 0.45$ for $D = 5$, and $V_0 = 0.275$ for $D = 10$. Again, the system forms a metastable layered structure at early times, which is broken up by spinodal fluctuations. (For very strong surface fields, the layered structure actually corresponds to an equilibrium state.) However, in this case, the B-rich regions are encapsulated by A. The asymptotic dynamics is characterized by the lateral coarsening of these encapsulated domains. The laterally averaged profiles (Fig. 10) again show that the system exhibits strong layering at early times (compare with Fig. 6). The depth profiles become softer at later times, but there remains a strong surface enrichment in A.

Figure 11 is a scaling plot of $C(\rho, t)/C(0, t)$ vs. ρ/L for $D = 10$, and is analogous to Fig. 8. (We do not show data for the $z = 0$ case here as the surface is always A-rich and does not exhibit interesting pattern dynamics.) The behavior in the film center ($z = 5$) is similar to the PW case, i.e., there is no dynamical scaling for the time-window shown. This can be understood in the context of the evolution dynamics shown in Fig. 9(b). For the $D = 10$ case, the morphologies exhibit a crossover behavior from the layered state to the asymptotic CW state for $t = 100, 1000, 20000$. For $t \geq 20000$, we expect to recover dynamical scaling.

In this case also, the behavior of $L(z, t)$ vs. t was found to exhibit a non-monotonic behavior [115]. The non-monotonic behavior again reflects the formation and break-up of a long-lived layered structure. The break-up of the layered structure leads to the growth of laterally segregated domains. This regime is expected to show LS growth in the late stages.

Finally, we compare the above continuum approach (based on a GL free-energy functional) with the molecular field theory [based on the appropriate generalization of (13)–(15)]. Since the continuum model is expected to reproduce the lattice theory if $\xi_b \gg a$, we present here the comparison for the borderline case $\xi_b/a = 1$. For the Ising model defined in (7), this means a choice of temperature $k_B T/J = 5.57$ [74]. Figure 12(a) shows the evolution of the averaged order parameter profiles across the film, comparing the continuum and lattice models for a choice of parameters where the models should agree precisely. Indeed one finds that the time evolution of the profiles according to both methods displays a great similarity. In fact, at $\xi_b/a = 2$ (reached for $k_B T/J = 5.875$) the curves according to both methods are already barely distinguishable [74]. However, at somewhat lower temperatures than shown here (e.g., $\xi_b/a = 1/2$ which is reached for $k_B T/J = 4.75$), there are already significant differences between the lattice approach and the continuum approach [see Fig. 12(b)].

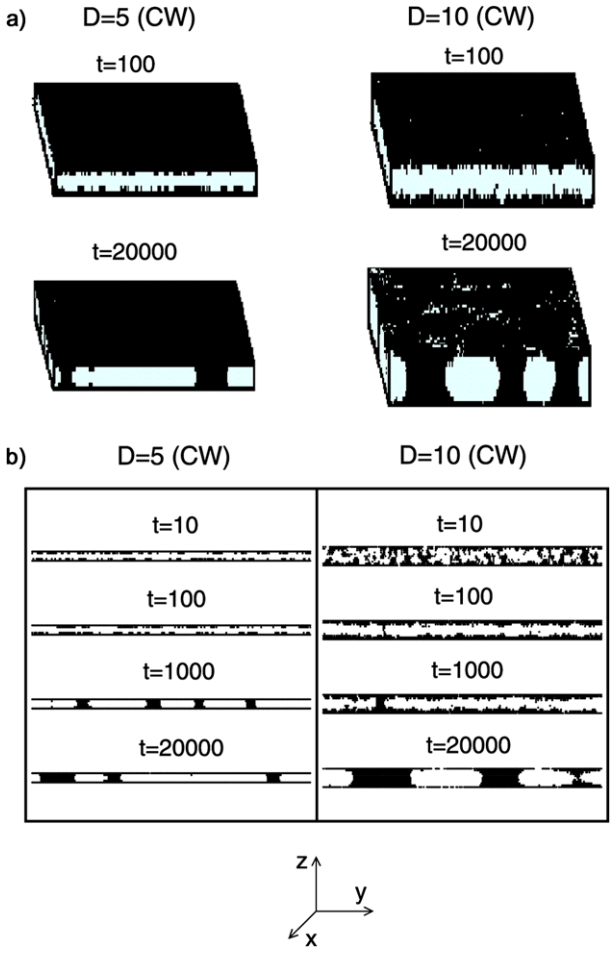

Fig. 9 Analogous to Fig. 5, but for a symmetric film with a CW morphology. The potential strengths were $V_0 = 0.45$ (for $D = 5$) and $V_0 = 0.275$ (for $D = 10$)

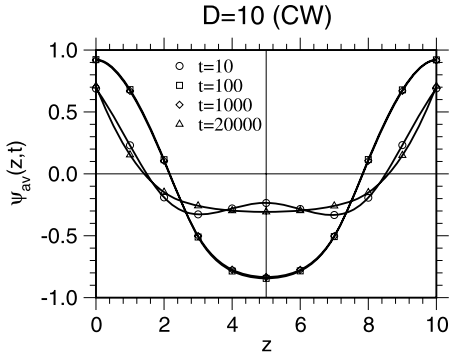

Fig. 10 Analogous to Fig. 6, but for the CW evolution depicted in Fig. 9

Of course, the advantage of the lattice approach is that it allows a study of SDSD for the Ising films at temperatures such as $k_B T/J = 4.0$ (Figs. 13–15), where the GL approach would no longer have any quantitative connection to the parameters of the Ising model. Fig-

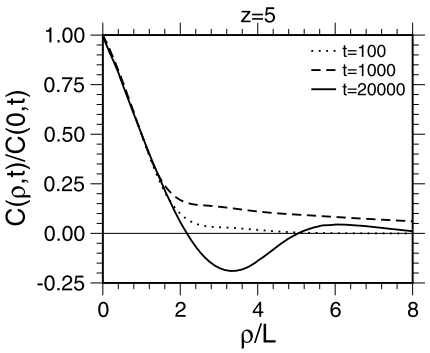

Fig. 11 Analogous to Fig. 8, but for the CW evolution depicted in Fig. 9. In this case, the $z = 0$ layer is always A-rich

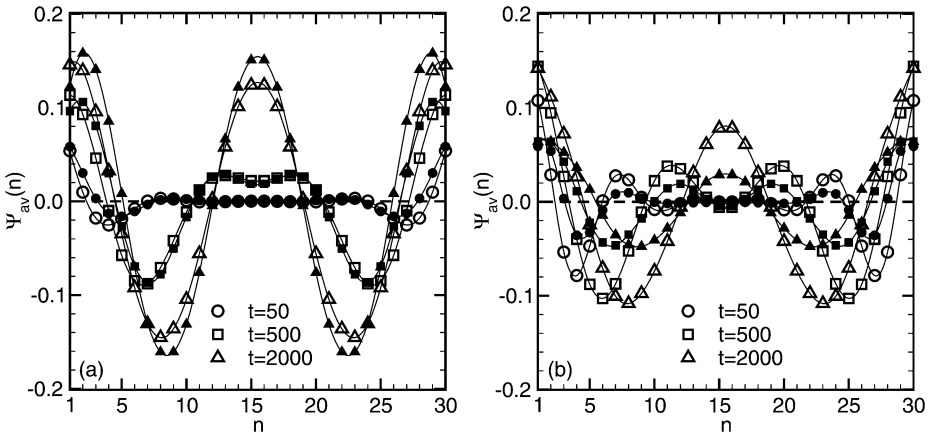

Fig. 12 (**a**) Plot of $\psi_{\rm av}(n)$ vs. n for an Ising thin film with 30 layers (labeled by n). The parameter values are $J_{\rm s} = J, k_B T/J = 5.57, H_1 = H_D = 0.1J$. The *open symbols* correspond to the lattice model, while the closed symbols denote the Ginzburg-Landau model. The initial configuration was a random spin configuration in both cases. Three times after the quench are shown, as indicated (**b**) same as (**a**), but for $k_B T/J = 4.75$. (From Das et al. [74])

ure 13 shows that one still sees the hallmarks of SDSD with the lattice model. From the initial state (broken horizontal line showing $\psi_{\rm av}(n, t = 0) = 0$) the system develops "damped concentration waves", driven by the growth of the order parameter at the surfaces, but the two waves interact in the center of the film. The profile finally resembles that of a layered structure. However, a glance at cross-sectional snapshots (Fig. 14) shows that the system exhibits lateral phase separation, with domains that steadily coarsen as the time increases, and Figs. 13(a), (b) only reflect the average surface enrichment (and adjacent depletion) effects when one averages over all these domains. For the thinnest film that has been studied (the distance $D = 9$ lattice spacings between the first and last layer means there are only 10 planes $n = 1, \ldots, 10$), it was possible to reach the very late stages. Here, the characteristic length scale of phase separation $L(n, t)$, defined in terms of the first zero crossing of $C_n(\rho, t)/C_n(0, t)$ in Fig. 15(a), exceeds D already. On this length scale, the order-parameter variation in the direction perpendicular to the walls is no longer important, and basically Figs. 14, 15 show spinodal decomposition in $d = 2$. One also finds that the length scale $L(n, t)$ for times $t < 10^3$ increases with time only rather slowly, and the behavior is not de-

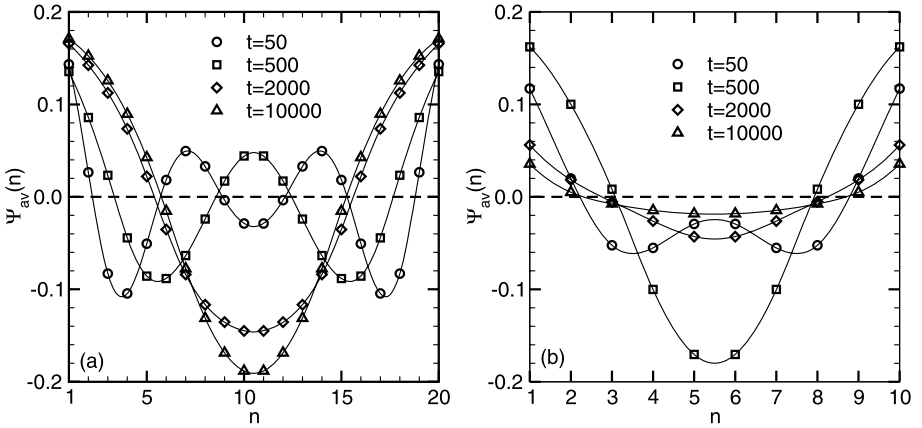

Fig. 13 (**a**) Layer-wise averaged order parameter profiles, $\psi_{\rm av}(n)$ vs. n, for four different times in the cases (**a**) $D = 19, L = 128$, and (**b**) $D = 9, L = 128$. The parameter values are $k_B T/J = 4.0$, $J_{\rm S}/J = 1$, $H_1 = H_D = 0.1J$. These results were obtained by solving (13)–(15) numerically with time unit $\tau_{\rm S} = 1$, time step $\Delta t = 0.1$. We averaged over 5 independent runs. (From Das et al. [74])

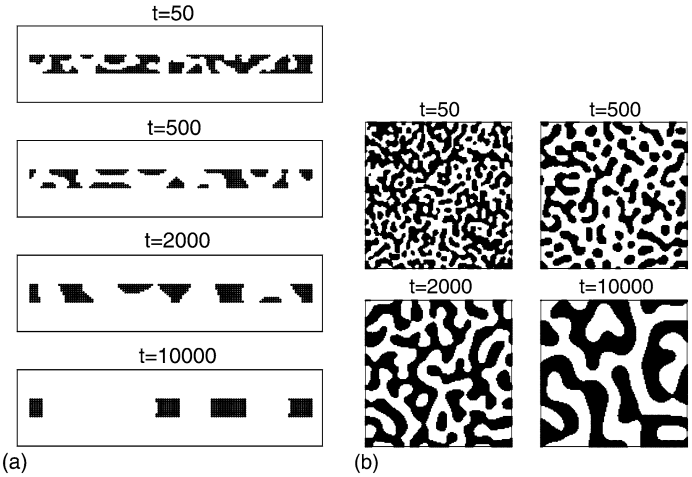

Fig. 14 Cross-sectional snapshots of the system with $D = 9$ (i.e., 10 layers), $L = 128$, $H_1/J = H_D/J = 0.1$, $J_s/J = 1, k_B T/J = 4.0$ for (**a**) the (xz)-plane and (**b**) the (xy)-plane in the center of the thin film ($n = 5$). (From Das et al. [74])

scribed by power law growth yet. Only for $t > 10^3$ does one find [74] a behavior of $L(n, t)$ roughly consistent with the LS law, expected to hold for the present model [1, 2].

4.3 Molecular Dynamics Simulation Results for a Confined Binary Lennard-Jones Mixture

As discussed in Sect. 2.2, hydrodynamic flows can drastically affect phase-separation kinetics. We have used MD techniques to study phase separation in a fluid mixture confined to a thin film geometry [116, 117]. The static behavior of this model is very similar to the behavior of a confined Ising system, but we expect the dynamical properties to be very different.

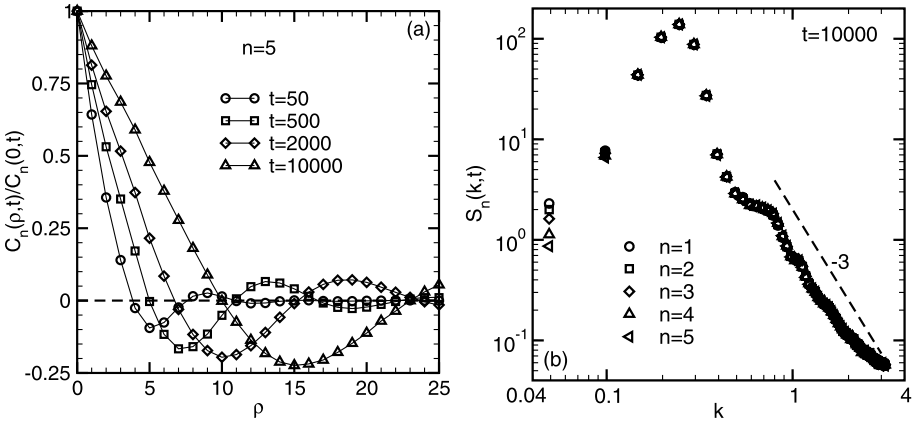

Fig. 15 (**a**) Correlation function $C_n(\rho,t)/C_n(0,t)$ for the spins in layer $n=5$ for the same system as in Fig. 14, and four times as indicated. (**b**) Fourier transform $S_n(k,t)$ of $C_n(\rho,t)$ plotted vs. k, resolved with respect to individual layers for the same system as shown in Fig. 14, and the time $t=10000$ after the quench. The *dashed line* corresponds to the $d=2$ Porod law, $S_n(k,t) \propto k^{-3}$. (From Das et al. [74])

Hence it is of interest to compare what is still similar to the behavior of Ising models and GL models, as considered above, and elucidate the consequences of hydrodynamics for phase separation in thin films. Recall that many of the experiments mentioned in the introduction [12, 13, 15–18] have been carried out for thin fluid polymer films.

We consider [116, 117] N_A A-atoms and N_B B-atoms ($N_A = N_B = N/2$) in a $L \times L \times D$ box with periodic boundary conditions in x- and y-directions. There are pairwise interactions between the particles given by standard Lennard-Jones potential:

$$u(r_{ij}) = 4\epsilon_{\alpha\beta}\left[\left(\frac{\sigma}{r_{ij}}\right)^{12} - \left(\frac{\sigma}{r_{ij}}\right)^{6} + C\right], \quad r_{ij} \le r_c = 2.5\sigma. \tag{53}$$

Here, $r_{ij} = |\vec{r}_i - \vec{r}_j|$ is the distance between the (point-like) particles i, j, $\alpha = $ A or B, and the constant C is chosen such that the potential is continuous for $r_{ij} = r_c$. The interaction energy scales are chosen as $\epsilon_{AA} = \epsilon_{BB} = \epsilon$ while $\epsilon_{AB} = \epsilon/2$, so the energy controlling unmixing is $\Delta\epsilon = (\epsilon_{AA} + \epsilon_{BB})/2 - \epsilon_{AB} = \epsilon/2$. The particle density is chosen as $n = N/(L^2 D) = 1$, choosing $\sigma = 1$ as the unit of length in this subsection. The walls at $z = 0$ and $z = D$ are characterized by the potential:

$$u_w(z) = \frac{2\pi n\sigma^3}{3}\epsilon_w\left[\frac{2}{15}\left(\frac{\sigma}{z'}\right)^9 - \delta_\alpha\left(\frac{\sigma}{z'}\right)^3\right], \tag{54}$$

with $\epsilon_w = 0.005\epsilon$ and $\delta_A = 1$, $\delta_B = 0$ (attractive forces act on A-particles only). The coordinate $z' = z + \sigma/2$ corresponds to the left wall at $z = 0$, and $z' = D - z + \sigma/2$ to the right wall at $z = D$. Standard velocity Verlet algorithms are used to integrate Newton's equation of motion, and temperature is kept constant by using a Nosé-Hoover thermostat [118]. For bulk phase behavior and dynamical properties of this symmetric binary model, without surfaces, see [119–121].

At the critical concentration $x = N_A/N = 1/2$, quenches from $T_0 = 5$ (choosing units such that $\epsilon/k_B = 1$) to $T = 1.1$ are performed (in the bulk, $T_c = 1.638$ for this model).

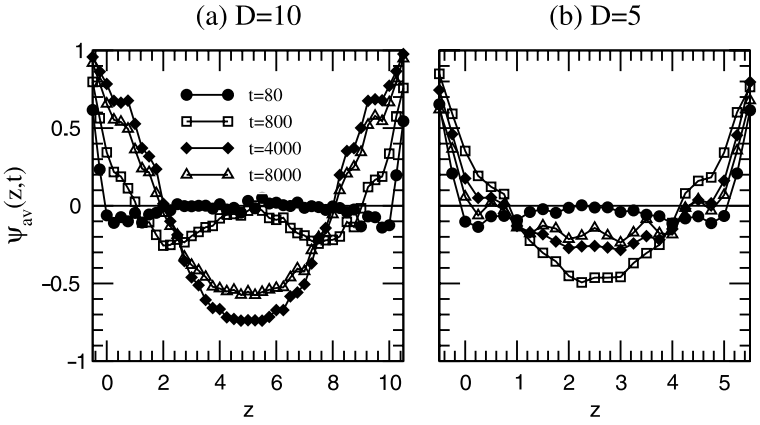

Fig. 16 Laterally averaged order parameter profiles, $\psi_{\rm av}(z,t)$ vs. z for (**a**) $D = 10, L = 64$, and (**b**) $D = 5, L = 128$. The times shown are $t = 80, 800, 4000$ and 8000, choosing standard MD time units $\tau = (m\sigma^2/48a)^{1/2} = 1/\sqrt{48}$. (From Das et al. [116, 117])

At T_0, attractive parts of both $u(r_{ij})$ and $u_{\rm w}(z)$ have little effect, so the initial distribution in the dense fluid corresponds to a random mixture. Figure 16 shows the evolution of the profiles of the local order parameter:

$$\psi_{\rm av}(z,t) = \frac{n_{\rm A}(z,t) - n_{\rm B}(z,t)}{n_{\rm A}(z,t) + n_{\rm B}(z,t)}, \tag{55}$$

defined in terms of the local densities $n_{\rm A}(z,t), n_{\rm B}(z,t)$ of A, B particles averaged in slices of width $\Delta z = 0.2$ in layers $L \times L \times \Delta z$ parallel to the walls. Clearly, the MD results are qualitatively similar to both the Ginzburg-Landau counterparts (Figs. 6, 10) and the lattice model (Fig. 13). Of course, a quantitative mapping cannot be expected, since the local packing of particles in a fluid clearly differs from the arrangement of a simple cubic Ising model. Further, the quench depths and wall potentials are also somewhat different. In spite of differences in detail, both the average profiles and the configuration snapshots (compare Fig. 17 with Fig. 14) are similar.

We again study the layer-wise order-parameter correlation function, and the corresponding length scale $L(z,t)$. For the times available in the simulation, no dynamic scaling was found. This lack of dynamical scaling correlates with the fact that the length $L(z,t)$ did not exhibit a simple power law behavior. For $t \leq 500$ MD time units, $L(z,t)$ is rather small, of the order of a few Lennard-Jones diameters only. At later times a crossover to a behavior compatible with $L(z,t) \propto t^{2/3}$ occurs. A theoretical explanation for this exponent in this regime of scales for length and times is lacking, however.

Although binary liquid mixtures that undergo phase separation in thin film geometry can exhibit growth of large scale structures with a characteristic length $L(z,t) \gg D$ only in two directions (x, y) parallel to the walls, one should not expect that the growth kinetics is identical to that of a strictly two-dimensional system. As we have discussed in Sect. 2.2, in $d = 3$ dimensions the coarsening of interconnected domain structures can proceed by a mechanism where an inhomogeneous velocity field is formed. In thin films, however, any velocity field must satisfy hydrodynamic boundary conditions at the walls. As is well-known, a standard formulation of such boundary conditions in thin fluid films between parallel solid walls (usually considered for the case of laterally uniform Poisseuille flow) uses the concept of a

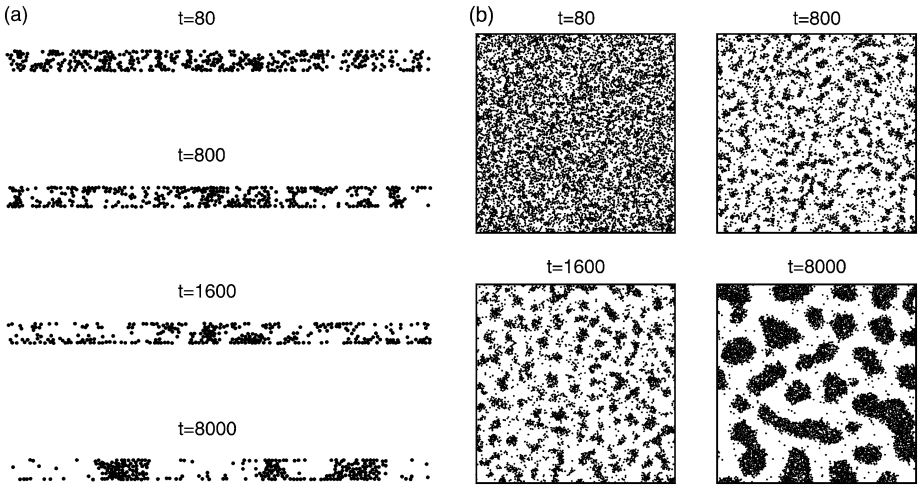

Fig. 17 (**a**) Snapshots of the concentration distribution in cross-sectional slices of linear dimensions $\sigma \times L \times D$ through the films for $D = 5$, centered at $x = D/2$. The A-particles are marked black, while the B-particles are not shown. The times of the snapshots are indicated. (**b**) Same as (**a**), but for a $L \times L \times 5$ cross-sectional slice centered at the mid-plane ($z = D/2$) of the film. (From Das et al. [116, 117])

"slip length", which in turn strongly depends on the wettability conditions of the walls for the binary fluid mixture. Depending on the film thickness, hydrodynamic mechanisms of coarsening hence are expected to be modified. In view of these speculative considerations, Das et al. [116, 117] made a comparative study of $L(z, t)$ for three choices of film thickness. Indeed it was found that the onset of power law growth (with an effective exponent near 2/3) occurs for $D = 20$ much faster (at about $t = 500$ MD time units) than for $D = 5$ (where it occurs only at about $t = 3000$ MD time units), in the central region of these films (near $z = D/2$). This observation indicates a gradual speed-up of the coarsening as D increases. Clearly, it would be very interesting to actually study the statistical properties of the fluctuating velocity filed during phase separation in the film, resolved as function of z and t. However, due to the very significant statistical effort needed for such a study this must be left to future work.

5 Summary and Discussion

In this paper, we reviewed the state of the art of simulations of surface-directed spinodal decomposition (SDSD) in binary mixtures. There has been extensive use of a phenomenological Ginzburg-Landau (GL) model, which corresponds to the Cahn-Hilliard-Cook (CHC) equation in the bulk, amended by suitable boundary conditions at the surface(s) [52, 53]. These boundary conditions are motivated by justifying the model as the continuum limit for the Kawasaki spin exchange Ising model on the simple cubic lattice, treating the latter in a local molecular field approximation. While in the latter the order parameter is a strictly conserved quantity, and apart from the molecular-field approximation no further approximations are made, the GL model is based on a simplified treatment of the boundary condition [(25), or even its static limit]. However, at least for the case of thin films confined symmetrically between equivalent walls, the GL treatment is found to be rather accurate if the correlation length exceeds the lattice spacing of the model.

A fairly general finding is that, near the surface of a semi-infinite system (as well as near both surfaces of a thin film), the growth of enrichment and depletion layers of the preferred phase shows a complicated interplay with the domain growth in the regions further away from the walls. As a consequence, the length scale $L(z,t)$, characterizing the linear dimension of A-rich domains a distance z from the surface, does not show a simple power-law behavior at the times accessible to our numerical simulations. The standard Lifshitz-Slyozov-like growth [$L(z,t) \propto t^{1/3}$] seems to take over only at very late times. Very interesting behavior also occurs for strongly off-critical quenches, where no phase separation occurs in the bulk, while wetting layers grow at the surfaces [see Fig. 3(c)]. The details of this behavior differ for long-range surface forces from the logarithmic growth law that is found for short-range surface forces. However, even now the behavior is well-understood only for the cases where either the surface is in the complete wetting regime, so layers can grow at the walls without the need of overcoming a nucleation barrier, or for the case where the system is brought into a state where the system is unstable in the bulk, so that bulk spinodal decomposition occurs and is affected by the surface effects.

Only recently the case where phase separation at walls and in thin films starts by the formation of critical nuclei has received attention, but this work has focused on free energy barriers rather than on the kinetics of phase separation [113, 114, 122]. A study of segregation kinetics in confined geometries triggered by heterogeneous nucleation of wall-attached droplets remains to be done in future work. Also the consequences of the gradual transition from spinodal decomposition to nucleation in the bulk, when the state to which the quench leads is located close to the spinodal curve, remains to be elucidated for SDSD.

This review has described the analytical arguments on the subject, and has also mentioned experiments very briefly. The reason for the lack of detailed discussion of experiments is simply that the molecular field kinetic Ising model, as well as the GL model, are only idealized caricatures of experiments, where normally thin fluid films of two kinds of (entangled) polymers on a substrate were considered [15–18]. These systems are (often rather asymmetric) fluid binary mixtures, and also the two surfaces (the bottom surface being a solid substrate, the top surface being a smooth interface against air) are non-equivalent. First steps to simulate fluid binary mixtures confined by symmetrical walls already showed that hydrodynamic effects change the behavior substantially, but the studied system (binary Lennard-Jones mixture with a strictly symmetric phase diagram in the bulk) is not a realistic model for such a polymer mixture. Clearly, many further refinements of the studied models will be necessary, before a serious attempt to compare the simulations to experiment is warranted.

Acknowledgements One of us (S.P.) acknowledges support from the Deutsche Forschungsgemeinschaft (DFG) under Sonderforschungsbereich (SFB) 625/A3, another (S.K.D.) from Sonderforschungsbereich TR6/A5.

References

1. Bray, A.J.: Adv. Phys. **43**, 357 (1994)
2. Binder, K., Fratzl, P.: In: Kostorz, G. (ed.) Phase Transformations in Materials, p. 409. Wiley, Weinheim (2001)
3. Onuki, A.: Phase Transition Dynamics. Cambridge University Press, Cambridge (2002)
4. Dattagupta, S., Puri, S.: Dissipative Phenomena in Condensed Matter: Some Applications. Springer, Heidelberg (2004)
5. Puri, S., Wadhawan, V.K. (eds.): Kinetics of Phase Transitions. CRC Press, Boca Raton (2009)
6. Young, T.: Philos. Trans. R. Soc. Lond., Ser. A **95**, 69 (1805)

7. Cahn, J.W.: J. Chem. Phys. **66**, 3667 (1977)
8. Fisher, M.E.: J. Stat. Phys. **34**, 667 (1984)
9. Fisher, M.E.: J. Chem. Soc. Faraday Trans. **282**, 1569 (1986)
10. de Gennes, P.G.: Rev. Mod. Phys. **57**, 827 (1985)
11. Dietrich, S.: In: Domb, C., Lebowitz, J.L. (eds.) Phase Transitions and Critical Phenomena, vol. 12, p. 1. Academic Press, London (1988)
12. Puri, S., Frisch, H.L.: J. Phys.: Condens. Matter **9**, 2109 (1997)
13. Puri, S.: J. Phys.: Condens. Matter **17**, R1 (2005)
14. Binder, K.: J. Non-Equilib. Thermodyn. **23**, 1 (1998)
15. Jones, R.A.L., Norton, L.J., Kramer, E.J., Bates, F.S., Wiltzius, P.: Phys. Rev. Lett. **66**, 1326 (1991)
16. Krausch, G., Dai, C.-A., Kramer, E.J., Bates, F.S.: Phys. Rev. Lett. **71**, 3669 (1993)
17. Krausch, G.: Mater. Sci. Eng. Rep. **R14**, 1 (1995)
18. Geoghegan, M., Krausch, G.: Prog. Polym. Sci. **28**, 261 (2003)
19. Lifshitz, I.M., Slyozov, V.V.: J. Phys. Chem. Solids **19**, 35 (1961)
20. Siggia, E.: Phys. Rev. A **20**, 595 (1979)
21. Miguel San, M., Grant, M., Gunton, J.D.: Phys. Rev. A **31**, 1001 (1985)
22. Furukawa, H.: Phys. Rev. A **31**, 1103 (1985)
23. Furukawa, H.: Phys. Rev. A **36**, 2288 (1987)
24. Furukawa, H.: Physica A **204**, 237 (1994)
25. Binder, K., Stauffer, D.: Phys. Rev. Lett. **33**, 1006 (1974)
26. Binder, K.: Phys. Rev. B **15**, 4425 (1977)
27. Huse, D.A.: Phys. Rev. B **34**, 7845 (1986)
28. Das, S.K., Puri, S.: Phys. Rev. E **65**, 026141 (2002)
29. Wagner, A.J., Yeomans, J.M.: Phys. Rev. Lett. **80**, 1429 (1998)
30. Furukawa, H.: Phys. Rev. E **61**, 1423 (2000)
31. Wagner, A.J., Cates, M.E.: Europhys. Lett. **56**, 556 (2001)
32. Farrell, J.E., Valls, O.T.: Phys. Rev. B **40**, 7027 (1989)
33. Farrell, J.E., Valls, O.T.: Phys. Rev. B **42**, 2353 (1990)
34. Farrell, J.E., Valls, O.T.: Phys. Rev. B **43**, 630 (1991)
35. Laradji, M., Toxvaerd, S., Mouritsen, O.G.: Phys. Rev. Lett. **77**, 2253 (1996)
36. Velasco, E., Toxvaerd, S.: Phys. Rev. Lett. **71**, 388 (1993)
37. Ossadnik, P., Gyure, M.F., Stanley, H.E., Glotzer, S.: Phys. Rev. Lett. **72**, 2498 (1994)
38. Diehl, H.W., Janssen, H.-K.: Phys. Rev. A **45**, 7140 (1992)
39. Sullivan, D.E., da Gama, M.M.T.: In: Croxton, C.A. (ed.) Fluid Interfacial Phenomena. Wiley, New York (1986), Chap. 2
40. Schick, M.: In: Charvolin, J., Joanny, J.-F., Zinn-Justin, J. (eds.) Liquids at Interfaces, p. 415. North-Holland, Amsterdam (1990)
41. Forgacs, G., Lipowsky, R., Nieuwenhuizen, T.M.: In: Domb, C., Lebowitz, J.L. (eds.) Phase Transitions and Critical Phenomena, vol. 14. Academic Press, London (1991), Chap. 2
42. Binder, K.: In: Pettifor, D.G. (ed.) Cohesion and Structure of Surfaces, p. 121. Elsevier Science, Amsterdam (1995)
43. Bonn, D., Ross, D.: Rep. Prog. Phys. **64**, 1085 (2001)
44. Telo da Gama, M.M.: In: Dünweg, B., Landau, D.P., Milchev, A.I. (eds.) Computer Simulations of Surfaces and Interfaces, p. 239. Kluwer Acad., Dordrecht (2003)
45. Binder, K., Landau, D.P., Müller, M.: J. Stat. Phys. **110**, 1411 (2003)
46. Binder, K.: In: Domb, C., Lebowitz, J.L. (eds.) Phase Transitions and Critical Phenomena, vol. 8, p. 1. Academic Press, London (1983)
47. Kawasaki, K.: In: Domb, C., Green, M.S. (eds.) Phase Transitions and Critical Phenomena, vol. 2, p. 443. Academic Press, London (1972)
48. Binder, K.: Z. Phys. **267**, 313 (1974)
49. Binder, K., Frischr, H.L.: Z. Phys. B **84**, 403 (1991)
50. Puri, S., Frisch, H.L.: J. Chem. Phys. **79**, 5560 (1993)
51. Frisch, H.L., Puri, S., Nielaba, P.: J. Chem. Phys. **110**, 10514 (1999)
52. Puri, S., Binder, K.: Phys. Rev. A **46**, R4487 (1992)
53. Puri, S., Binder, K.: Phys. Rev. E **49**, 5359 (1994)
54. Ball, R.C., Essery, R.L.H.: J. Phys.: Condens. Matter **2**, 10303 (1990)
55. Hohenberg, P.C., Halperin, B.I.: Rev. Mod. Phys. **49**, 435 (1977)
56. Schmidt, I., Binder, K.: Z. Phys. B **67**, 369 (1987)
57. Puri, S., Binder, K.: Z. Phys. B **86**, 263 (1992)
58. Tanaka, H.: J. Phys.: Condens. Matter **13**, 4637 (2001)
59. Dzyaloshinskii, I.E., Lifshitz, E.M., Pitaevskii, L.P.: Adv. Phys. **10**, 165 (1961)

60. Oono, Y., Puri, S.: Phys. Rev. Lett. **58**, 836 (1987)
61. Oono, Y., Puri, S.: Phys. Rev. A **38**, 434 (1988)
62. Puri, S., Oono, Y.: Phys. Rev. A **38**, 1542 (1988)
63. Puri, S.: Phys. Lett. A **134**, 205 (1988)
64. Puri, S., Binder, K.: Phys. Rev. Lett. **86**, 1797 (2001)
65. Puri, S., Binder, K.: Phys. Rev. E **66**, 061602 (2002)
66. Puri, S., Binder, K., Frisch, H.L.: Phys. Rev. E **56**, 6991 (1997)
67. Brown, G., Chakrabarti, A.: Phys. Rev. A **46**, 4829 (1992)
68. Marko, J.F.: Phys. Rev. E **48**, 2861 (1993)
69. Karim, A., Douglas, J.F., Lee, B.P., Glotzer, S.C., Rogers, J.A., Jackman, R.J., Amis, E.J., Whitesides, G.M.: Phys. Rev. E **57**, R6273 (1998)
70. Lee, B.P., Douglas, J.F., Glotzer, S.C.: Phys. Rev. E **60**, 5812 (1999)
71. Jaiswal, P., Puri, S.: In preparation
72. Yan, L.-T., Xie, X.M.: J. Chem. Phys. **128**, 034901 (2008)
73. Yan, L.-T., Li, J., Xie, X.M.: J. Chem. Phys. **128**, 224906 (2008)
74. Das, S.K., Horbach, J., Binder, K.: Phys. Rev. E **79**, 021602 (2009)
75. Henderson, I.C., Clarke, N.: Macromol. Theory Simul. **14**, 435 (2005)
76. Fukuda, J.-I., Yoneya, M., Yokoyama, H.: Phys. Rev. E **73**, 066706 (2006)
77. Binder, K., Das, S.K., Horbach, J.: Mod. Phys. Lett. B **23**, 549 (2009)
78. Marro, J., Bortz, A.B., Kalos, M.H., Lebowitz, J.L.: Phys. Rev. B **12**, 2000 (1975)
79. Amar, J.G., Sullivan, F.E., Mountain, R.D.: Phys. Rev. B **37**, 196 (1988)
80. Marko, J.F., Barkema, G.T.: Phys. Rev. E **52**, 2522 (1995)
81. Majumder, S., Das, S.K.: Unpublished
82. Yaldram, K., Binder, K.: J. Stat. Phys. **62**, 161 (1991)
83. Puri, S.: Phys. Rev. E **55**, 1752 (1997)
84. Puri, S., Sharma, R.: Phys. Rev. E **57**, 1873 (1998)
85. Martin, G., Bellon, P.: Solid State Phys. **50**, 189 (1997)
86. Puri, S., Binder, K.: J. Stat. Phys. **77**, 145 (1994)
87. Liu, A.J., Durian, D.J., Herbolzheimer, E., Safran, S.A.: Phys. Rev. Lett. **65**, 1897 (1990)
88. Monette, L., Liu, A.J., Grest, G.S.: Phys. Rev. A **46**, 7664 (1992)
89. Bhattacharya, A., Rao, M., Chakrabarti, A.: Phys. Rev. E **49**, 524 (1994)
90. Vaksman, M.A., McMullen, W.E.: Phys. Rev. E **49**, 4724 (1994)
91. Liu, J., Wu, X., Lennard, W.N., Landheer, D.: Phys. Rev. B **80**, 041403(R) (2009)
92. Fisher, M.E., Nakanishi, H.: J. Chem. Phys. **75**, 5857 (1981)
93. Nakanishi, H., Fisher, M.E.: J. Chem. Phys. **78**, 3279 (1983)
94. Evans, R., Tarazona, P.: Phys. Rev. Lett. **52**, 557 (1984)
95. Nicolaides, D., Evans, R.: Phys. Rev. B **39**, 9336 (1989)
96. Evans, R.: J. Phys.: Condens. Matter **2**, 8989 (1990)
97. Binder, K., Landau, D.P.: J. Chem. Phys. **96**, 1444 (1992)
98. Binder, K.: Ann. Rev. Phys. Chem. **43**, 33 (1992)
99. Rouault, Y., Baschnagel, J., Binder, K.: J. Stat. Phys. **80**, 1009 (1995)
100. Flebbe, T., Dünweg, B., Binder, K.: J. Phys. II (France) **6**, 667 (1996)
101. Binder, K., Nielaba, P., Pereyra, V.: Z. Phys. B **104**, 81 (1997)
102. Müller, M., Binder, K.: Macromolecules **31**, 8323 (1998)
103. Fisher, M.E.: Rev. Mod. Phys. **46**, 597 (1974)
104. Binder, K., Luitjen, E.: Phys. Rep. **344**, 179 (2001)
105. Gelb, L.D., Gubbins, K.E., Radhakrishnan, R., Slivinska-Bartkowiak, M.: Rep. Prog. Phys. **62**, 1573 (1999)
106. Kroll, D.M., Gompper, G.: Phys. Rev. B **39**, 433 (1989)
107. Indekeu, J.O.: Int. J. Mod. Phys. **138**, 309 (1994)
108. Drelich, J.: Colloids Surf. A **116**, 43 (1996)
109. Getta, T., Dietrich, S.: Phys. Rev. E **57**, 655 (1998)
110. Bauer, C., Dietrich, S.: Eur. Phys. J. B **10**, 767 (1999)
111. Milchev, A., Binder, K.: J. Chem. Phys. **114**, 8610 (2001)
112. MacDowell, L.G., Müller, M., Binder, K.: Coll. Surf. A **206**, 277 (2002)
113. Winter, D., Virnau, P., Binder, K.: J. Phys.: Condens. Matter **21**, 464118 (2009)
114. Winter, D., Virnau, P., Binder, K.: Phys. Rev. Lett. **103**, 225703 (2009)
115. Das, S.K., Puri, S., Horbach, J., Binder, K.: Phys. Rev. E **72**, 061603 (2005)
116. Das, S.K., Puri, S., Horbach, J., Binder, K.: Phys. Rev. E **73**, 031604 (2006)

117. Das, S.K., Puri, S., Horbach, J., Binder, K.: Phys. Rev. Lett. **96**, 016107 (2006)
118. Allen, M.P., Tildesley, D.J.: Computer Simulation of Liquids. Clarendon, Oxford (1987)
119. Das, S.K., Horbach, J., Binder, K.: J. Chem. Phys. **119**, 1547 (2003)
120. Das, S.K., Horbach, J., Binder, K., Fisher, M.E., Sengers, J.V.: J. Chem. Phys. **125**, 024506 (2006)
121. Das, S.K., Fisher, M.E., Sengers, J.V., Horbach, J., Binder, K.: Phys. Rev. Lett. **97**, 025702 (2006)
122. Qiu, C., Qian, T., Ren, W.: J. Chem. Phys. **129**, 154711 (2008)